PREPARATION OF DRUG LOADED ALBUMIN NANOPARTICLES IN WATER / IONIC LIQUIDS MICROEMULSION SYSTEMS

A Thesis Submitted to
the Graduate School of
İzmir Institute of Technology
in Partial Fulfillment of the Requirements for the Degree of

MASTER OF SCIENCE

In Material Science and Engineering

by

Barış YILDIRIM

December 2021

IZMIR

ACKNOWLEDGEMENTS

I would like to thank my thesis advisor Assoc. Prof. Dr. Yaşar AKDOĞAN for his guidance and for sharing his knowledge and experience with me.

Also, I would like to thank other members of the thesis committee, Assoc. Prof. Dr. Fatih TOPTAN and Asst. Prof. Dr. Muhammed ÜÇÜNCÜ for their valuable comments and suggestions.

I would like to thank scientists at the Center for Materials Research of IZTECH for SEM analysis. I would like to thank the TUBITAK (118Z341) for supporting me during the project. I would like to thank DEMİR's Lab for DLS analysis.

And last, I wish to thank all my colleagues, lab mates Remziye YILDIZ, Sümeyra Çiğdem SÖZER, Tuğçe EGESOY, Begüm DEMİRKURT and my friends Alper İNAN and Dilek TEPELİ for their endless support and courage on each step of this journey.

I would like to express my gratitude to Melih ARAT for always being with me, encouraging me, his endless support, and being a home to me.

ABSTRACT

PREPARATION OF DRUG LOADED ALBUMIN NANOPARTICLES IN WATER / IONIC LIQUIDS MICROEMULSION SYSTEMS

Nanoparticles (NPs) have been used in various applications such as biotechnology, nanomedicine, and drug delivery systems. Many nanoparticle drug delivery systems have been promoted for cancer treatment, and numerous materials have been investigated to use as drug delivery agents to enhance the therapeutic efficiency and safety of anticancer drugs. Albumin is a natural biopolymer and the most abundant protein in blood plasma. Due to its versatile binding capacity of widespread therapeutical drugs, albumin becomes an ideal material to obtain nanoparticles.

In this study, the ionic liquid (IL) based emulsification methods were investigated. Instead of classical toxic and volatile solvents, using ILs in microemulsions, environment-friendly media were received to synthesize bovine serum albumin (BSA) NPs. In order to obtain BSA NPs, high-speed homogenizer processing was applied by following crosslinker addition.

The IL microemulsions are a thermodynamically stable colloidal dispersion containing spherical droplets (W/IL or IL/W) in submicron sizes that act as nanoreactors for NP formation. Chlorambucil (CHL) was used as a model drug to investigate drug loading and releasing kinetics of BSA NPs as a drug delivery candidate. Results showed that chlorambucil loading capacities and release kinetics depended on the synthesized medium such as anion-type of ILs and surfactants. CHL loaded to the BSA NPs synthesized in hydrophilic IL BmimBF$_4$ in relatively higher amounts and released in the same trend. In addition, the cell viability effect of CHL-loaded BSA NPs synthesized in different types of ILs were investigated. The CHL-loaded BSA NPs synthesized in BmimOTf and BmimPF$_6$ reduced the cancer cell viability more than the used same dose of free CHL.

ÖZET

İLAÇ YÜKLÜ ALBUMİN NANOPARÇACIKLARININ SU/İYONİK SIVI MİKROEMÜLSİYON SİSTEMLERİNDE HAZIRLANMASI

Nanoparçacıklar (NPs), biyoteknoloji, nanotıp ve ilaç taşıyıcı sistemler gibi çeşitli uygulamalarda kullanılmaktadır. Örneğin, kanser tedavisi için çeşitli nanoparçacık ilaç taşıma sistemleri geliştirilmiş ve antikanser ilaçların terapötik verimliliği ve güvenli uygulamalarını artırmak için ilaç taşıma ajanları olarak kullanmak üzere çok sayıda malzeme araştırılmıştır. Protein albümin, kan plazmasındaki en bol bulunan proteindir. Yaygın terapötik ilaçlara çok yönlü bağlanabilme kapasitesinden dolayı albumin nanoparçacık üretmek için ideal bir malzemedir.

Bu çalışmada iyonik sıvı (IL) bazlı emülsifikasyon yöntemleri araştırılmıştır. Bovine serum albumin (BSA) NP'larını sentezlemek için klasik olarak kullanılan toksik ve uçucu çözücüler yerine, mikroemülsiyonlarda IL'lerin kullanıldığı çevre dostu bir mediyum kullanılmıştır. BSA NP'leri elde etmek için yüksek hızlı homojenizatör ile birlikte çapraz-bağlayıcı ilave edilmiştir.

IL mikroemülsiyonları, NP oluşumu için nanoreaktörler olarak işlev gören mikron altı boyutlarda küresel damlacıklar (W/IL veya IL/W) içeren termodinamik olarak kararlı kolloidal bir yapıdır. Klorambusil (CHL), BSA NP'ların ilaç taşıma adayı olara, ilaç yüklenme ve salınım kinetiğini araştırmak için model ilaç olarak kullanılmıştır. Sonuçlar, klorambusil yüklenme kapasitelerinin ve salınım kinetiğinin, sentezlendiği ortamdaki IL'in anyon tipine ve yüzey aktif maddeye bağlı olduğunu göstermiştir. CHL, hidrofilik IL, $BmimBF_4$'te sentezlenen BSA NP'larına nispeten daha yüksek miktarlarda yüklenmiş ve aynı eğilimde salınım gerekleştirmiştir. Ek olarak, farklı tip IL'lerde sentezlenen CHL yüklü BSA NP'larının hücre canlılığına olan etkileri araştırılmış ve BmimOTf ve $BmimPF_6$'da sentezlenen BSA NP'ları, aynı doz kullanılan serbest CHL'ya karşı kanser hücrelerinin canlılığını daha fazla düşürmüştür.

TABLE OF CONTENTS

LIST OF FIGURES

Figure **Page**

Figure **Page**

Figure **Page**

Figure **Page**

LIST OF TABLES

Table **Page**

CHAPTER 1

INTRODUCTION

1.1. Nanoparticle Based Drug Delivery Systems

Nanoparticle-based drug delivery systems are products of a relatively new nanomedicine field, a discipline between medicine and nanotechnology. The advantages of nanoparticles as a drug delivery system have been a significant advance on fundamental properties of drugs such as diffusivity, solubility, half-life in the blood circulatory system, and drug-releasing kinetics.[1] Nanoparticles can improve the solubility and stability of encapsulated drugs. Thus, the neglected drug candidates in the past because of inadequate pharmacokinetics can reconsider. Besides, nanoscale drug delivery can transport a variety of therapeutics and diagnostics such as hydrophilic and hydrophobic small molecules, peptides, proteins, nucleic acids, etc. In designing the nanoparticles as drug carriers, the main objectives that regulate the system's efficiency are surface properties, particle size distribution, adsorption, and release kinetics of pharmaceuticals.[2]

Table 1.1. Marketed nano-systems for cancer treatment [2]

Product name	Drug	Type of nanocarrier	Company
Daunoxome	Daunorubicin citrate	Liposome	Gilead Science, Cambridge, UK
Doxil	Doxorubicin HCl	Liposome	Johnson and Johnson, NJ, USA
Myocet	Doxorubicin	Liposome	SopherionTherapeutics, NJ, USA
Caelyx	Doxorubicin HCl	Pegylated liposome	Johnson and Johnson, NJ, USA
Transdrug	Doxorubicin	Poly(alkylcyanoacrylate) nanoparticles	BioAlliance, Paris, France
Genexol-PM	Paclitaxel	Methoxy-PEG-polylactide nanoparticles	Samyang, South Korea
Oncaspar	Pegaspargase	PEG-asparaginase nanoparticles	Enzon, NJ, USA
Abraxane	Paclitaxel	Albumin-bound nanoparticles	American Bioscience, CA, USA

Various types of nanomaterial-based drugs have already been taking place for pharmaceutical uses commercially. Some examples of commercial nano-systems pharmaceuticals for cancer treatment are listed in table 1.1.

Nanoparticles can be synthesized from metals, ceramics, and polymers (synthetic or natural-based) for pharmaceutical applications (Figure 1.1.). Polymeric particles have been studied as nanocarriers of pharmaceutical molecules and genes.[1] The main disadvantages of polymeric-based nanoparticles are relatively low drug loading capacities and wider size distribution than metal and ceramic-based nanoparticles. Besides that, polymeric nanoparticles can be obtained in a variation of sizes and morphology, which allows sustaining localized drugs for more extended periods. Natural polymers, also known as biopolymers, exhibit some extra advantages besides the typical advantages of polymer-based nanoparticles, such as their inherited biocompatibility and biodegradability, less immune response, and astonishing binding capacities for some drugs. [3]

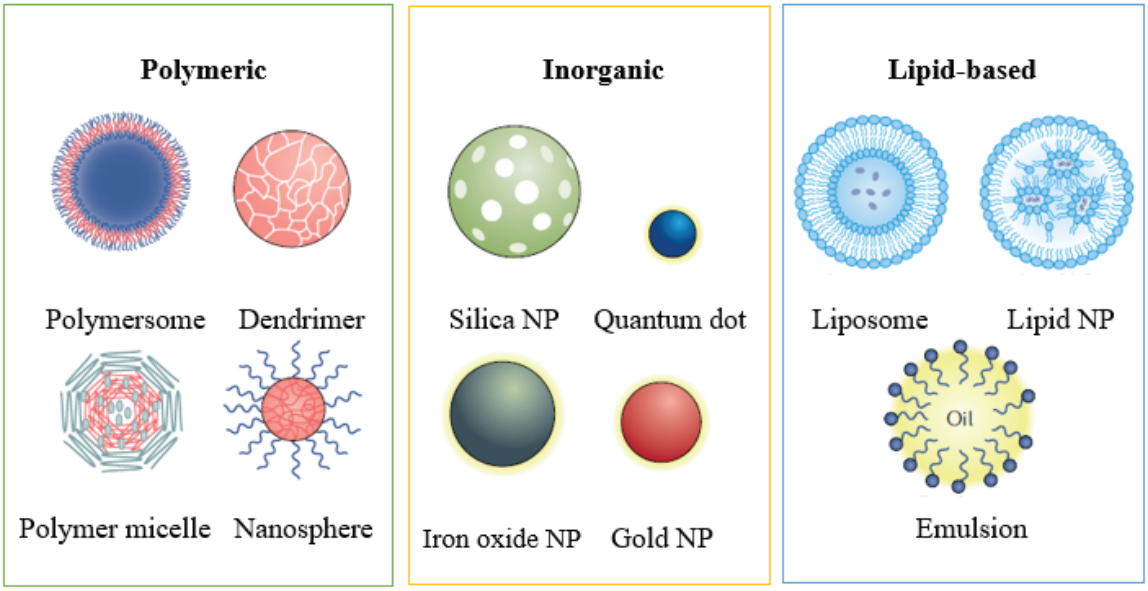

Figure 1.1. Classes of NPs. Each class of nanoparticle (NP) features multiple subclasses, with some of the most common ones were schematized here.[4]

In the literature, drug delivery systems have been developed to increase the treatment efficiency of drugs. For example, in the study of Ahmed et al., the natural biopolymers, alginate-chitosan NPs, were synthesized by the W/O nano-emulsification method and coated with the drug rabeprazole.[4] They used nanoparticles to enhance the

bioactivity of the drug and by aiming to increase in efficiency of the treatment. Another study indicated that natural polymer silk fibroin was used to obtain curcumin-loaded nanoparticles to increase the anticancer efficiency of curcumin. First, the silk fibroin proteins were stabilized in ionic liquids, and then nanoparticles were obtained by spray drying method.[5]

1.2. Albumin As a Nanocarrier for Drug Delivery

Albumin is the most widespread protein in the blood plasma, and 60% of all proteins in the blood comprise it. Albumin is highly soluble in water, and it is a small globular protein with a weight of 67 kDa.

One of the main roles of albumin is to retain the intravascular colloid osmotic pressure. As an inherent property, it carries hydrophobic molecules (such hormones and as fatty acids), transports therapeutical agents, and neutralizes toxins. Hence, its versatile binding capacity makes the albumin is a suitable candidate for drug delivery.[6,7]

As a plasma protein, albumin is natural, versatile nanocarrier utilizing a high binding capacity for hydrophobic and hydrophilic bioactive molecules, besides minimal immunogenicity and toxicity, particularly in targeting local treatments.[8] Due to these extraordinary capabilities, albumin has inspired scientists to develop albumin-based nanocarriers.

Albumin can be isolated from various sources for biomedical applications, the most common ones; Human Serum Albumin (HSA), Bovine Serum Albumin (BSA), rat serum albumin (RAS), and ovalbumin (OVA). Similar to human-sourced one, BSA (Figure 1.2.) is widely used for drug delivery due to its abundance, biocompatibility, biodegradability, water-solubility, and low cost. Also, being homologous to human serum albumin (76% homologous sequence), BSA becomes an excellent material for this purpose.[8,9]

BSA involves 583 amino acids within homologous I, II, III domains to each other and the subdomains IIA and IIIA (Sudlow's sites I and II) well-characterized binding sites.[9]

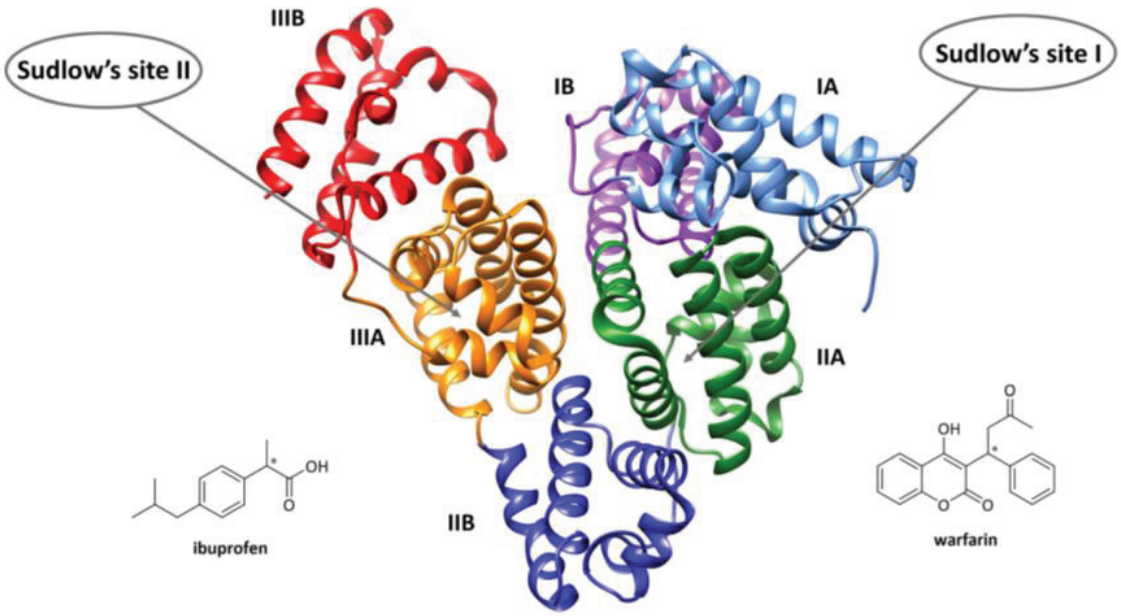

Figure 1.2. Bovine serum albumin (BSA), the two major drug binding sites (Sudlow's sites I and II) and the respective site-markers (warfarin, site I; ibuprofen, site II). Domains are color-coded (light blue, IA; purple, IB; green, IIA; blue, IIB; orange, IIIA; red, IIIB).[10]

Several techniques can be used to fabricate albumin-based NPs. They can be categorized as chemical and physical base techniques. The chemical based methods, desolvation, emulsification, and self-assembly methods are the most common ones.[11] Within these techniques, the desolvation method is the most broadly used technique in the formation of albumin NPs. In the desolvation methods, adding the coacervating agent (usually ethanol, acetone, or acetonitrile) to the pH-adjusted albumin solution changes the tertiary structure of albumin by increasing hydrophobicity and forming submicron aggregates.[12–14] The size distribution and uniformity of the synthesized nanoparticles can be controlled by changing pH, ionic strength, albumin concentration, etc. The desolvation method allows a designable, repeatable, and appropriate method to obtain albumin NPs. The emulsification technique involves the emulsification of albumin solution in a continuous lipophilic phase and solidification by chemical crosslinker or thermal denaturation.[15,16] The requirement to use organic solvents, purification steps to eliminate the oily phase and surfactants, difficulty in controlling the albumin NPs size distribution limit the emulsification method.[11]

1.3. Ionic Liquids (ILs)

Ionic liquids are a kind of salt that consists of an organic cation and polyatomic inorganic anion. ILs are generally liquid at room temperature and are called molten salts.[17] The first molten salt, ethylammonium nitrate, was discovered a century ago in 1914 by German chemist Walden.[18] However, it was not counted as a widespread solvent in chemical applications during the years. Organic chloroaluminates, accepted as the first generation of ILs, were first mentioned in 1951 in the literature, and their properties were investigated in detail for the next twenty years. In the '90s, air and water-stable ionic liquids were obtained within the diversity of ions combinations. The science of ionic liquids has proceeded following the days of their discovery. They have been marked by exponential growth, especially in the last 30 years. Today, IL research is a genuinely interdisciplinary field between physic, chemistry, biology, computational sciences, and engineering applications. Moreover, the novel variability of the ions enables design regarding desired applications.[19,20] The most common cations and anions in IL research are shown in Figure 1.3.

Ionic liquids can be classified as hydrophilic and hydrophobic, depending on the solubility in an aqueous medium. Anion and cation variations determine the intermolecular interactions of the ionic liquids.[19] As a consequence of this, ionic liquids can be miscible or immiscible with water.[21]

Ionic liquids can be brilliant for dissolving biopolymers and developing biomaterials because of their designability by combining different anions and cations. Green solvent features like non-volatility, inflammability, and recyclability make them safe, easy to use, and environment-friendly solvent systems.

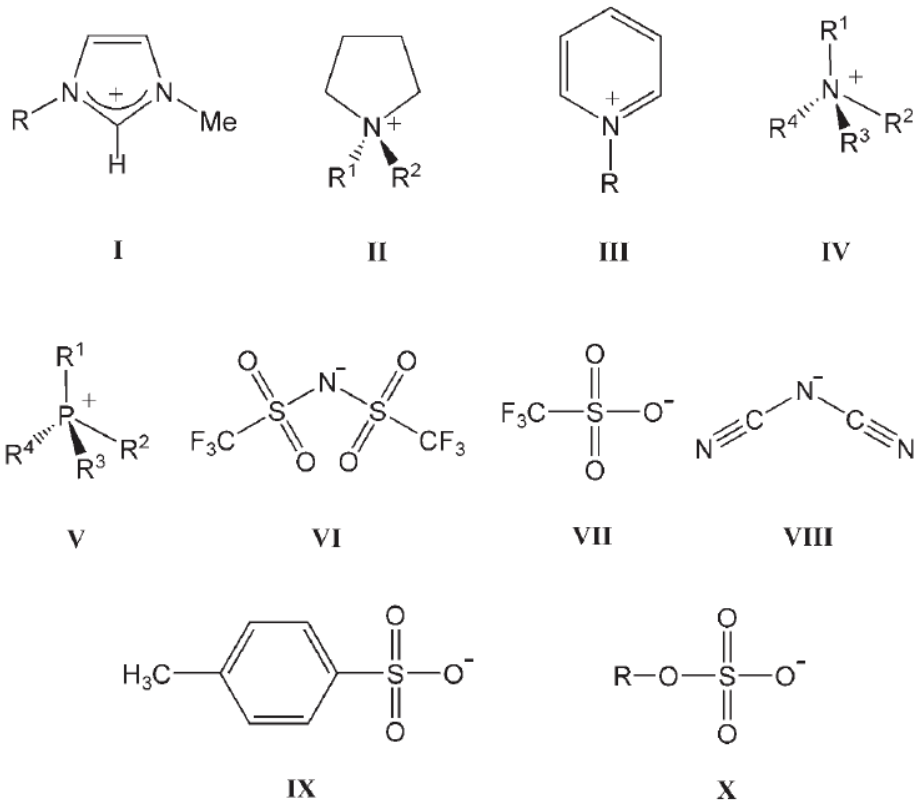

Figure 1.3. The most common anions and cations in IL science: **I**: 1-alkyl-3 methylimidazolium ($[C_nmim]^+$, C_n stands for *n*-alkyl residues C_nH_{n+1}); **II**: 1,1-dialkylpyrrolidinium ($[C_mC_npyr]^+$); **III:** 1-alkylpyridinium ($[C_npy]^+$); **IV**: tetraalkylammonium ($[N_{ijkl}]^+$); **V**: tetraalkylphosphonium ($[P_{ijkl}]^+$); **VI**: bis(trifluoromethanesulfonyl) amide ($[NTf_2]^-$); **VII:** trifluoromethanesulfonate ($[OTf]^-$); **VIII**: dicyanimide ($[(CN)_2N]^-$); **IX**: tosylate ($[OTos]^-$); **X**: alkylsulfates ($[C_nOSO_3]^-$).

In the last decades, ILs have been used to obtain films, scaffolds, membranes fibers, and nanoparticles from biopolymers such as cellulose, starch silk fibroin, keratin, xylan, chitosan, and heparin.[17,22] Some superior features of ILs against classical solvents are;

- Low surface tension advances to high nucleation rates.
- ILs are highly structured liquids due to their anionic and cationic components, and they heighten the electronic and steric stabilization of NPs. So, this prohibits particle growth by occurring negative and positive charge shells [23] (Figure 1.4.).

- The choice of IL in the synthesis of NPs affects the water solubility and the molecular affinity of the particles.

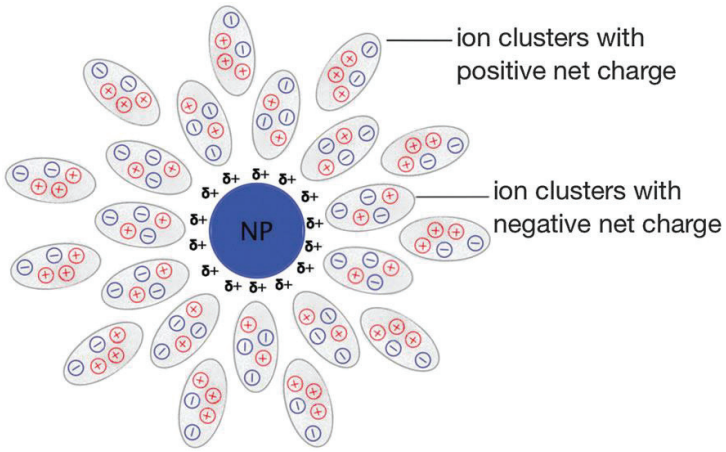

Figure 1.4. Schematic of ion clusters surrounding nanoparticles. The ion clusters form a protective electrical double layer. [23]

1.4. Ionic Liquid Microemulsions

Ionic liquid microemulsions, similarly classical microemulsions, could be obtained from two immiscible liquids (polar and nonpolar phase), stabilized by tertiary surface-active substances. They are thermodynamically stable, translucent, and isotropic systems and can be grouped into four categories as water-in-IL (W/IL), bicontinuous (BC), IL-in-water (IL/W), and non-equilibrated phase (Figure 1.5.).[24–26]

Surfactants, the stabilizing agents of a microemulsion, consist of two main entities, a hydrophilic head group and a hydrophobic (lipophilic) tail group. The hydrophilic and hydrophobic heads of the surfactants form soft aggregates in solvent (or continuous phase), efficiently disperse the cores, and offer rooms for particle nucleation while preventing aggregation of the obtained NPs. Reverse micelles, which behave as nanoreactors for nanoparticle growth, form in the W/O region (or W/IL) of microemulsions. Surfactants held continuous phase, nanocores, and formed nanoparticles together by van der Waals and ionic forces.[26]

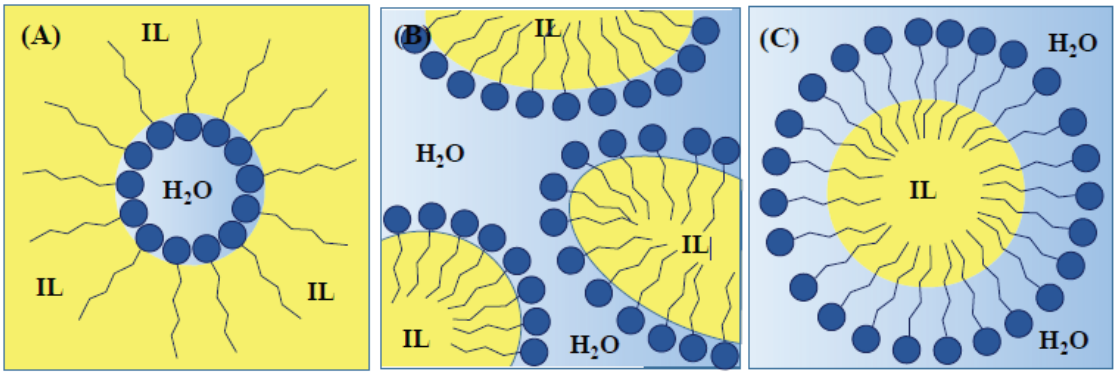

Figure 1.5. Schematic representation of the microemulsion systems: (A) water/ionic liquid (W/IL), (B) bicontinuous (BC), (C) ionic liquid/water (IL/W).[24]

In the literature, IL microemulsions have been used to synthesize NPs. For instance, Demirkurt et al. revealed a W/IL microemulsion system consisting of $BmimPF_6$/Tween 20/water microemulsion to synthesize BSA NPs, in ~200 nm size and -11 mV surface charge, as an alternative classical organic volatile solvents method.[15] In another study, Zhou et al. reported 91 nm-sized starch NPs, synthesized through the W/IL region of $BmiPF_6$/TX-100/1-butanol/water microemulsion system. The starch nanoparticles were tested as a drug carrier candidate, and entrapment efficiencies were found in the range of 11.54 and 16.55% regarding obtained starch nanoparticle size distribution.[27]

1.5. Chlorambucil

Chlorambucil (4-[bis(chloroethyl)amino]benzenebutanoic acid) (Figure 1.6.) is an alkylating antineoplastic drug used in blood cancer (leukemia), lymph cancer, and Hodgkin lymphoma.[28] Alkylating agents are used in many cancer treatments. As a result of DNA alkylation, DNA replication is inhibited, and thus the proliferation of the cancerous cell is stopped.

Chlorambucil (CHL) is a lipophilic anticancer drug, and it is insoluble in water but soluble in DMSO (dimethyl sulfoxide), ethanol, methanol, and acetonitrile. The use of CHL in clinical applications is limited because of its low solubility in water, chemical instability, and severe side effects.[29] The developed nanoparticle drug delivery systems can overcome these challenges.[30]

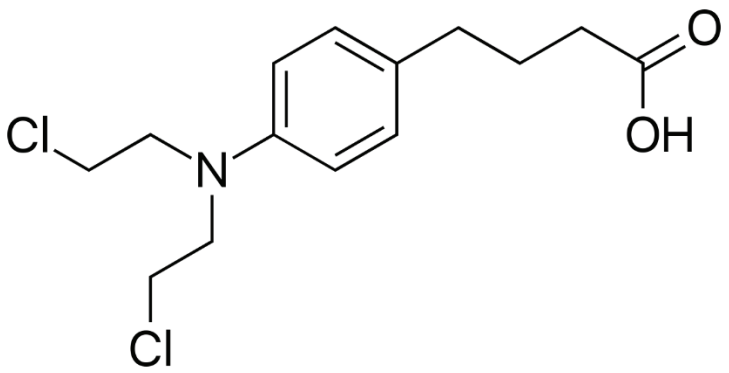

Figure 1.6. Chlorambucil structure

Chlorambucil could bind to albumin at a maximum of 2 sites.[31] Saufi et al. show that BSA interaction with CHL implies both hydrophobic interactions and hydrogen bonds. Besides, subdomain III-A was identified as the preferred binding site for CHL in this research.[9]

In addition, chlorambucil-containing albumin nanoparticles have been obtained in recent years, and their drug transport and release properties have been studied.[32] In the literature, the desolvation-ultrasonication method was used, and drug-loaded-albumin nanoparticles were obtained by adding the chlorambucil and ethanol-containing egg yolk lecithin to the water containing BSA. They found the entrapment efficiencies 65-86% to their lipoprotein-mimic nanoparticles in their research.[33] In another study, a microemulsion system using a high-pressure homogenizer was used. A mixture of chlorambucil, surfactant (E80), and soybean oil dissolved in DCM and water containing BSA were mixed using a high-pressure homogenizer to get chlorambucil containing lipid-albumin hybrid nanoparticles. In their developed lipid-BSA hybrid model nanoparticles, entrapment efficiencies were found as 88-91%.[34]

1.6. The Scope of the Thesis

Albumin nanoparticles are frequently used in drug delivery applications due to their various flexibility. However, the known and applicable production methods, such as desolvation and self-assembly, these techniques involve volatile, flammable, and toxic organic solvents, which may cause undesired health and environmental problems. IL-based methods offer safer and environment-friendly synthesis options. This study used an IL-based microemulsion system by replacing the nonpolar phase with hydrophobic IL

$BmimNTf_2$ to obtain BSA NPs. The single-phase and multi-phase boundaries of microemulsion were determined optically by water titration in defined IL/surfactant ratios. Conductivity measurements identified water-in-$BmimNTf_2$, bicontinuous, and $BmimNTf_2$-in-water subregions. In addition, the region of microemulsion (surfactant/IL ratio), surfactant, and co-surfactant effects on BSA NPs size distribution were investigated.

Many drugs bear severe difficulties concerning insolubility, instability in biological environments, inadequate uptake into cells and tissues, poor selectivity for targets, and undesired side effects. Nanoparticles can be designed as drug delivery systems to overwhelm many of these disadvantages.[8] ILs known as green solvents also have a good solvating ability for a diversity of molecules. As an insoluble drug in an aqueous medium, chlorambucil was chosen as a model drug for investigations. Drug loading ad releasing capacities of BSA NPs synthesized in the hydrophilic ILs, $BmimBF_4$ and BmimOTf, and the hydrophobic ILs, $BmimNTf_2$, and $BmimPF_6$ were investigated. Due to the UV-active benzamine group of the chlorambucil, UV-Vis spectrometry was used to determine unbound and released CHL molecules from the nanoparticles. Thus, with the help of the UV-vis absorbance data, drug loading capacities and releasing kinetics of BSA NPs were determined.

Cell cytotoxicity of chosen BSA NPs synthesized in $BmimPF_6$ and BmimOTf systems were investigated in four cancer cell lines. This information was used to prove the efficiency of drug delivery of BSA NPs.

CHAPTER 2

MATERIALS AND METHODS

2.1. Materials

BSA (M.W.= 66.000 Da, lyophilized powder), [BMIM][BF_4] (1-Butyl-3-methylimidazolium tetrafluoroborate*)*, [BMIM][PF_6], (1-Butyl-3-methylimidazolium hexafluorophosphate*),* [BMIM][NTf_2] (1-Butyl-3-methylimidazolium bis (trifluoromethanesulfonyl)imide), [BMIM][OTf] (1-Butyl-3-methylimidazolium trifluoromethanesulfonate) (Figure 2.1.), Triton™ X – 100, Tween™ 20, 1 – butanol, Glutaraldehyde solution (Grade II, 25% in H_2O), and absolute ethanol, methanol, 1-propanol were purchased from Sigma – Aldrich. All chemicals and solvents were analytical grade and used without any further purification processes. All aqueous solutions were prepared in Milli-Q water. The pH of aqueous solutions was adjusted with 0.1 M NaOH using an OHAUS STARTER3100 pH meter.

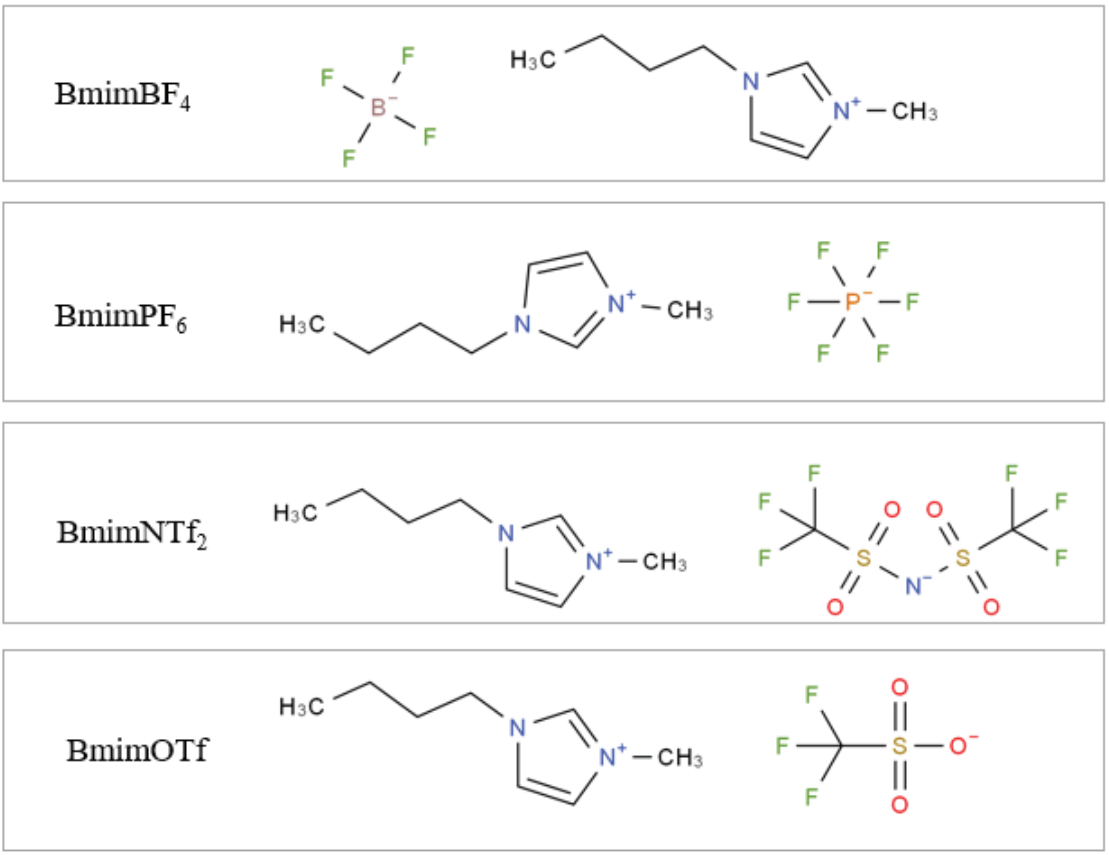

Figure 2.1. Ionic liquids and their chemical structures, which were investigated in the scope of the thesis. $BmimBF_4$: 1-Butyl-3-methylimidazolium tetrafluoroborate, $BmimPF_6$: 1-Butyl-3-methylimidazolium hexafluorophosphate, $BmimNTf_2$: 1-Butyl-3-methylimidazolium bis(trifluoromethanesulfonyl)imide, BmimOTf: 1-Butyl-3-methylimidazolium trifluoromethanesulfonate.

2.2. Preparation of BSA NPs

2.2.1. Preparation of BSA NPs in Hydrophilic ILs $BmimBF_4$ and BmimOTf

3 g of $BmimBF_4$, 90 mg of Triton X-100 (surfactant), and 30 mg of 1-butanol (co-surfactant) were stirred 15 minutes in a vial at 1,200 rpm. Next, 12 mg BSA containing 240 µL BSA solution at pH=9 was added dropwise to the mixture. Finally, 60 µL 25% (v/v) aqueous glutaraldehyde (crosslinker) solution was added to the total solution and immediately stirred at 22,000 rpm for 3 minutes by homogenizer (IKA T18, TURRAX).

By following that, the mixture was stirred for 15 minutes on a magnetic stirrer at 1,200 rpm to reach the thermodynamic equilibrium. After that, the suspension of nanoparticles was centrifuged at 10,000 rpm for 15 minutes. The experimental procedure of BSA NP synthesis was schematized in figure 2.2. The supernatant of the suspension was decanted carefully, and 50% (v/v) ethanol-water mixture was added to the centrifuge tubes for the resuspension process. Flocculated nanoparticle pellets were suspended with the help of vortex for 2-3 minutes and sonic bath for 15-20 minutes. Nanoparticles were washed twice with 50% (v/v) ethanol-water mixture and three times with ultra-pure water to eliminate IL, surfactant, co-surfactant, unreacted BSA, and glutaraldehyde by the repeating flocculation-suspension cycle. Within this procedure, BSA NPs formation yield was found 71%. After all, nanoparticles were prepared for further characterization analyses.

For BmimOTf/TX-100 system synthesis, 3 mg BmimOTf, 90 mg TX-100, and 30 mg 1-butanol were stirred 15 minutes in a vial at 1,200 rpm. Next, 15 mg BSA containing 480 µL BSA solution at pH=9 was added dropwise to the mixture. After then, 75 µL 25% (v/v) aqueous glutaraldehyde (crosslinker) solution was added to the total solution and immediately stirred at 15,000 rpm for 3 minutes by homogenizer (IKA T18, TURRAX). After that, the suspension of BSA NPs was stirred for 15 minutes. Purification steps were followed like described in the $BmimBF_4$ system. Within this procedure, BSA NPs formation yield was found 72%.

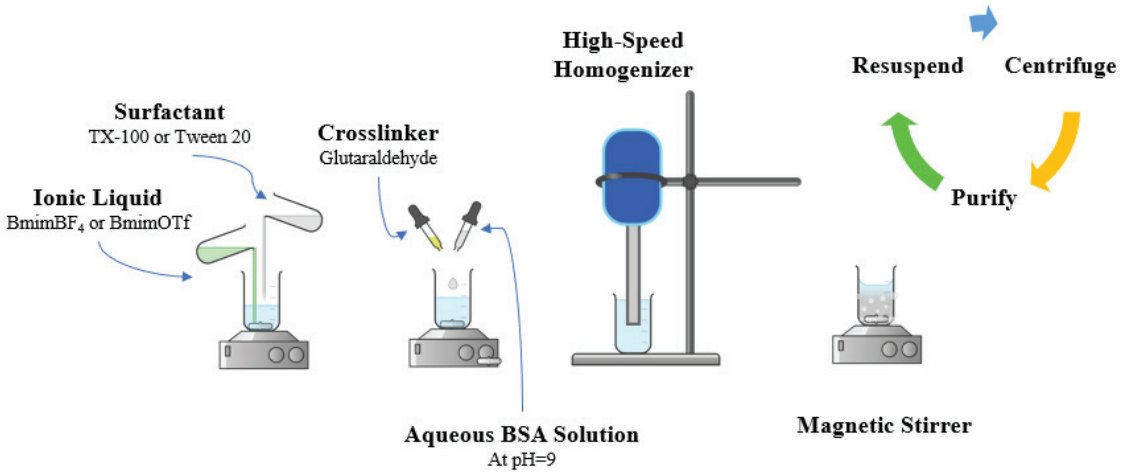

Figure 2.2. Schematic representation of BSA NP synthesis procedure in hydrophilic ILs ($BmimBF_4$ and BmimOTf).

2.2.2. Preparation of BSA Nanoparticles in Hydrophobic ILs $BmimPF_6$ and $BmimNTf_2$

BSA NPs were synthesized by using microemulsion cores of the W/IL system and a high-speed homogenizer. Glutaraldehyde was used as a crosslinker.

1,125 mg $BmimPF_6$ and 1,250 mg TX-100 (surfactant) were mixed for 15 minutes at 1,200 rpm. First, 10 mg BSA containing 125 μL BSA solution (pH=9) was added dropwise to the mixture and stirred at the same speed for 90 minutes. Then, the high-speed homogenizer was applied at 22,000 rpm for 3 minutes. Next, 45 μL 25% (v/v) aqueous glutaraldehyde (crosslinker) solution was added to the solution to obtain stable nanoparticles. The mixture was stirred overnight. To break the microemulsion, approximately 4 mL methanol was added and stirred for 15 minutes at 1,200 rpm. Next, the mixture was centrifuged at 1,200 rpm for 15 minutes. The supernatant of the suspension was decanted carefully, and a 50% (v/v) ethanol-water mixture was added to the centrifuge tubes for the resuspension process. Flocculated nanoparticle pellets were suspended with the help of vortex for 2-3 minutes and bath sonicator for 15-20 minutes. Nanoparticles were washed twice with 50% (v/v) ethanol-water mixture and three times with ultra-pure water to eliminate IL, surfactant, unreacted BSA, and glutaraldehyde by the repeating flocculation-suspension cycle. Within this procedure, BSA NPs formation yield was found 72%. After all, nanoparticles were prepared for further characterization analyses.

1,050 mg $BmimNTf_2$ and 1,800 mg TX-100 (surfactant) were mixed for 15 minutes at 1,200 rpm. First, 12 mg BSA containing 150 μL BSA solution (pH=9) was added dropwise to the mixture and stirred at the same speed for 90 minutes. Then, the homogenizer was applied at 22,000 rpm for 3 minutes. Next, 36 μL 25% (v/v) aqueous glutaraldehyde (crosslinker) solution was added to the solution to get solidified nanoparticles. The mixture was stirred overnight. To break the microemulsion, approximately 5 mL methanol was added and stirred for 15 minutes at 1,200 rpm. Finally, purification steps were followed as described for the $BmimPF_6$ system. Within this procedure, BSA NPs formation yield was found 71%. The experimental procedure of BSA NP synthesis in hydrophobic ILs were schematized in figure 2.3.

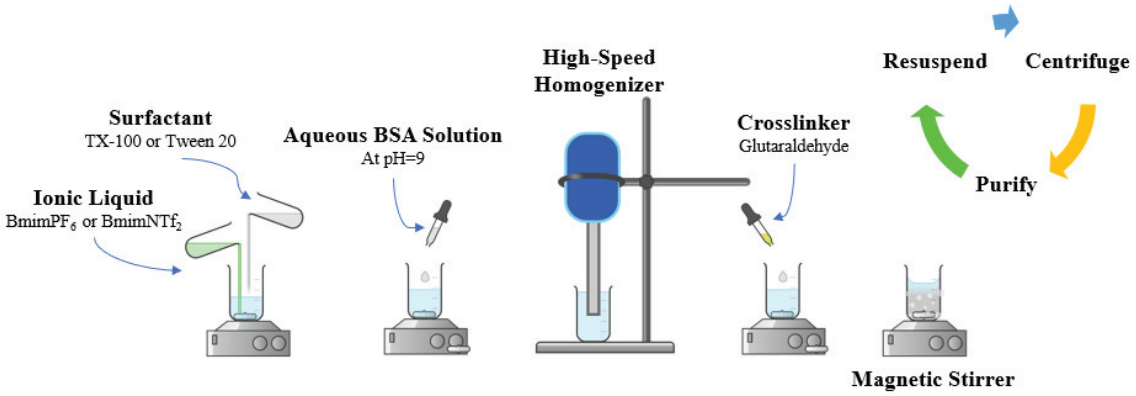

Figure 2.3. Schematic representation of BSA NP synthesis procedure in hydrophobic ILs ($BmimPF_6$ and $BmimNTf_2$).

2.2.3. Characterization of BSA NPs

The pellet of the nanoparticles was resuspended in 1.5 mL ultra-pure water (Milli-Q). The NPs suspension was diluted 1,000 times for Scanning Electron Microscopy (SEM) analysis. Diluted samples were suspended with the help of a sonicator bath for 20 minutes to prevent any aggregation of nanoparticles. Then, 10 µL nanoparticles suspension were dropped on a 500 mm^2 aluminum foil and placed in a fume hood to dry overnight. Samples were coated with gold before SEM analysis. Then, samples were analyzed by FEI QUANTA 250 FEG equipped with Everhart-Thornley Detector (ETD), collecting secondary electrons in 5 kV at the Center for Materials Research IZTECH. The size of the nanoparticles was determined by the scale bar o SEM images.

For size and zeta potential characterization, the pellet of the nanoparticles was resuspended in 1.5 mL ultra-pure water (Milli-Q). The NPs suspension was diluted approximately 1,000 times depending on the nanoparticle concentration. 1 mL of nanoparticles suspension was analyzed by Malvern dynamic light scattering Nano-ZS using disposable plastic cuvettes and suitable zeta charge cuvettes.

2.3. Drug Loading of Nanoparticles

Drug loading studies were adopted in two different methods. Firstly, the drug chlorambucil was added during the synthesis of nanoparticles. Secondly, chlorambucil was incubated with synthesized nanoparticles.

Chlorambucil is soluble in DMSO-water. Therefore, two types of DMSO-water mixtures were used, 1% and 15% (v/v) of DMSO.

2.3.1. BSA-CHL Solution

1 M CHL solution was prepared in DMSO and was used as a stock solution. The stock solution was diluted regarding the BSA concentration and mol ratio (such as 1:1, 1:2, 1:3, or 1:4, BSA:CHL).

BSA was dissolved in water as described amounts in related parts. The pH of the solution was adjusted to 9.0 by adding 0.1 M NaOH solution. Diluted CHL solutions were added to the BSA solution under constant shaking to prevent BSA denaturation. (DMSO content should be less than 3% (v/v) in the final BSA-CHL solution.)

2.3.2. Nanoparticle Synthesis with Chlorambucil in $BmimBF_4$ and BmimOTf systems

Similar methods of BSA NP synthesis (Part 2.2.1) with minor modifications were applied for synthesizing CHL-loaded BSA NPs. DMSO was used to dissolve CHL in the system at 1% (v/v). The CHL-BSA solution was used instead of the BSA solution in part 2.3.1.

3 g of BmimOTf, 90 mg of Triton X-100 (surfactant), 30 mg of 1-butanol (co-surfactant), and 28 µL DMSO were stirred 15 minutes in a vial at 1,200 rpm. 15 mg BSA containing 480 µL BSA -CHL solution (2,7% (v/v) DMSO) and 75 µL 25% (wt.%) glutaraldehyde were added dropwise to the mixture and immediately stirred at 15,000 rpm by homogenizer for 3 minutes. By following that, the mixture was stirred 15 minutes more on a magnetic stirrer at 1,200 rpm to reach the thermodynamic equilibrium. (BSA concentration was 0.8×10^{-4} M, and CHL concentrations were 0.8×10^{-4} M, 1.6×10^{-4} M, 2.4×10^{-4} M, and 3.2×10^{-4} M in the final mixture.)

3 g of $BmimBF_4$, 90 mg of Triton X-100 (surfactant), 30 mg of 1-butanol (co-surfactant), and 28 µL DMSO were stirred 15 minutes in a vial at 1,200 rpm. 12 mg BSA containing 240 µL BSA -CHL solution (2,7% (v/v) DMSO) and 60 µL 25% (wt.%) glutaraldehyde were added dropwise to the mixture and immediately stirred at 22,000 rpm by homogenizer for 3 minutes. By following that, the mixture was stirred 15 minutes

more on a magnetic stirrer at 1,200 rpm to reach the thermodynamic equilibrium. (BSA concentration was 0.62 x 10^{-4} M, and CHL concentrations were 0.62 x 10^{-4} M, 1.24 x 10^{-4} M, 1.86 x 10^{-4} M, and 2.48 x 10^{-4} M in the final mixture.)

After all that, the suspension of nanoparticles was centrifuged at 10,000 rpm for 15 minutes. Then, supernatants were decanted to another tube and separated for UV-Vis spectroscopy analysis to detect CHL quantity. Finally, the drug loaded BSA NP pellet was saved for further investigations.

2.3.3. Nanoparticle Synthesis with Chlorambucil in $BmimPF_6$ and $BmimNTf_2$ systems

3 g $BmimNTf_2$/TX-100/water microemulsion was prepared in 35:60:5 wt.% including 26 μL DMSO. 12 mg BSA in 150 μL water and CHL with various mol ratios were prepared as described in part 2.3.1 and were added dropwise to the mixture. They were mixed at 1,200 rpm on a magnetic stirrer for 90 minutes. By the flowing that, they were stirred at 22,000 rpm for 2 minutes by a homogenizer. 36 μL glutaraldehyde (25% (v/v) in H_2O) was added, and the system was stirred overnight at 1,200 rpm. A 5.2 mL of methanol was added to the system and precipitated nanoparticles were separated by centrifuge at 10,000 rpm for 15 minutes. (BSA concentration was 0.7 x 10^{-4} M, and CHL concentrations were 0.7 x 10^{-4} M, 1.4 x 10^{-4} M, 2.1 x 10^{-4} M, and 2.8 x 10^{-4} M in the final mixture.)

2.5 g $BmimPF_6$/TX-100/water microemulsion was prepared in 45:50:5 wt.% including 21.4 μL DMSO. 10 mg BSA in 125 μL water and CHL with various mol ratios were prepared like in part 2.3.1 and added dropwise to the mixture. They were mixed at 1,200 rpm on a magnetic stirrer for 90 minutes. By the flowing that, they were stirred at 22,000 rpm for 2 minutes by a high-speed homogenizer. 45 μL glutaraldehyde (25% (v/v) in H_2O) was added, and the system was stirred overnight at 1,200 rpm. A 4.28 mL of methanol was added to the system and precipitated nanoparticles were separated by centrifuge at 10,000 rpm for 15 minutes. (BSA concentration was 0.7 x 10^{-4} M, and CHL concentrations were 0.7 x 10^{-4} M, 1.4 x 10^{-4} M, 2.1 x 10^{-4} M, and 2.8 x 10^{-4} M in the final mixture.)

Supernatants were decanted to another tube and separated for UV-Vis spectroscopy analysis to detect CHL quantity. Finally, the drug loaded BSA NP pellet was saved for further investigations.

2.3.4. Drug Loading by Adsorption Method

BSA NPs, synthesized from different IL-Surfactant systems, were obtained as described in parts 2.2.1 and 2.2.2. After all purification steps, BSA NPs were suspended until getting a uniform blurry suspension in 1 mL ultrapure water with the help of a vortex and bath sonicator. The determined amount of CHL was diluted from stock solution to 1 mL %30 (v/v) DMSO-water solution by regards to 1:2, 1:10, 1:15, 1:20, and 1:25 (BSA:CHL) mole ratios (BSA concentration was 3.2 x 10^{-5} M in final mixture). 1 mL of BSA NP suspension and 1 mL of CHL solution were mixed and incubated for 24 hours under continuous shaking. Next, the supernatants were separated for UV-Vis analysis to determine the unbound CHL quantity.

The following formulas were used to calculate drug loading capacities and entrapment efficiencies.

$$Drug\ Entrapment\ Efficiency\ \% = \frac{Initial\ drug\ amount - Drug\ amount\ in\ supernatant}{Initial\ drug\ amount}\ x\ 100 \quad (1)$$

$$Drug\ Loading\ \% = \frac{Initial\ drug\ amount - Drug\ amount\ in\ supernatant}{Amount\ of\ BSA\ NP}\ x\ 100 \quad (2)$$

2.3.5. Drug Releasing of CHL Loaded BSA NPs

In vitro drug release of CHL loaded BSA NPs was performed in phosphate buffer (PB). (0.1 M, pH=7.4). Drug loaded BSA NPs were suspended in 800 µL ultrapure water ad placed into Merck© Milipore Mini dialysis tube. The dialysis tube was placed at 37 °C in the 34 mL PB under 750 rpm constant stirring. 2 mL of samples were taken from the PB in determined periods, and the samples were analyzed by UV-Vis spectrometer to detect released CHL content.

Quantitative CHL measurements were conducted by the calibration curve of known concentrations of CHL in PB, which were analyzed by UV-Vis spectrometer regarding absorbance intensities at 304 nm. The curve equation of the concentration versus absorbance intensity of CHL is Y=0.00251 + 0.9789 x C, R^2=0.999, (Y: signal magnitude, C: concertation).

2.3.6. In Vitro Studies and Cell Cytotoxicity

The cytotoxicity tests were tested by MTT (3-[4,5-dimethylthiazol-2-yl]-2,5-diphenyltetrazolium bromide, tetrazole) method. The cells were seeded to a 96-well plate as 7000 cells/well and incubated 24 hours at 37.5 °C for adherence. For CHL dose testing, 0 (control), 10,20,40, 80, 160, and 320 µM CHL including DMEM (Dulbecco's Modified Eagle Medium)-DMSO solution to be 1% (v/v) DMSO in the final medium concentration were incubated 48 hours with prepared cell cultures. After that, cell mediums were decanted, and 15 µL MTT (5 mg/mL) and 75 µL DMEM were added to each well, and cells were incubated for 4 hours. The cell mediums were separated by the following, and 100 µL DMSO (as solubilization solution) was added to dissolve the purple formazan crystals that occurred in the viable cells' mitochondria. Spectro-photometrical absorbances were performed by Thermo Scientific™ Multiskan™ GO Microplate Spectrophotometer at 570 nm. T-test was used to determine a significant difference between the means of two groups.

2.3.7. Cell Uptake and Imaging

Huh7 cells were cultured at 37 °C in 5% CO_2 in DMEM and 10% FBS. The fluorescent DiI ((2Z)-2-[(E)-3-(3,3-dimethyl-1-octadecylindol-1-ium-2-yl)prop-2-enylidene]-3,3-dimethyl-1-octadecylindole; perchlorate) dye was used to stain cell membranes for confocal microscopy analysis. 500,000 cells were washed with PBS (phosphate buffer saline) and incubated in 2.5 µL DiI including 50 µL PBS for 20 minutes in a 37 °C incubator. The cells were washed once with FBS (fetal bovine serum), twice with PBS, and resuspended in 5 mL DMEM. The cells were seeded as 50,000 cells/well in 8-well chamber slides. The next day 0.1 mg/mL FITC-BSA NPs were added and incubated 4 hours and 24 hours for cellular uptake tests. Cells were washed with PBS and

fixed with 4% PFA (paraformaldehyde). Next, the cells were washed with PBS, and the cell nuclei were stained with 4 μg/mL DAPI (diamidino-2-phenylindole) solution for 5 minutes. Finally, slides were mounted with 80% glycerol and were imaged with the Zeiss LSM880 Confocal microscope using a 63× oil objective. Image processing was done with FIJI software.

2.4. Phase Diagram

$BmimNTf_2$ and Tween 20 were mixed in various ratios (9:1, 8:2, 7:3, 6:4, 5:5, 4:6, 3:7, 2:8, and 1:9), and water was added systematically until getting a transparent single-phase emulsion. Depending on the added water amount, phase boundaries of the emulsion between single-phase and two-phase were determined. Conductivity measurements were performed to determine IL/W, bicontinuous, and W/IL subregions. $BmimNTf_2$ and Tween 20 were mixed in specific compositions (rates: 17:3, 9:1, and 19:1), and the mixture was titrated by water systemically. After water addition to the mixture, conductivities were measured by Thermo, Orion 3-star conductometer. Conductivity increased directly in proportion to the water content regarding the subregion of the microemulsion. Depending on the increasing rate of conductivity change, the subregions were determined (Figure 3.2.).

CHAPTER 3

RESULTS AND DISCUSSION

Ionic liquids can be miscible or immiscible in water as a consequence of anion and cation types.[21] The hydrophilic ILs, $BmimBF_4$, and BmimOTf are readily miscible with water, while hydrophobic ILs, $BmimPF_6$, and $BmimNTf_2$ are immiscible. Synthesis of BSA NPs in the systems of $BmimBF_4$ and $BmimPF_6$ have been studied by our research group.[15,35] In addition to these systems, we synthesized BSA NPs in the BmimOTf and $BminNTf_2$ systems.

For hydrophilic ILs, a clear solution forms with the mixture of water. Even though the solution of IL-water is macroscopically mixed, at the molecular level, water pools occur because of micelle-like characteristics of $BmimBF_4$.[36–38] On the other hand, hydrophobic ILs are not dissolved in an aqueous solution and do not form a single phase. Yet, surfactants are used as a ternary component to get a single-phase uniform mixture.

In the classical method of microemulsion formation, microemulsions consist of oil phase, water phase, and surface-active molecules. In this method, the oil phase was substituted with ILs.

3.1. Synthesis and Characterization of BSA NPs

3.1.1. Synthesis and Characterization of BSA NPs in the BmimOTf System

BSA NPs were obtained in the hydrophilic BmimOTf IL system as described in part 2.2.1. In addition, the purified BSA NPs were characterized by dynamic light scattering (DLS) and scanning electron microscopy (SEM), as described in part 2.2.3.

According to the SEM images, nanoparticle morphology is dominantly spherical and in the 175-250 nm size range. However, DLS results provided a broader particle size distribution between 350 and 700 nm (Figure 3.1.). While SEM analysis was done by using dried nanoparticles, DLS measurements were performed in a nanoparticle-water

dispersion. The swelling of nanoparticles in an aqueous medium and measured hydrodynamic radius can be the reason for obtaining larger results by DLS.

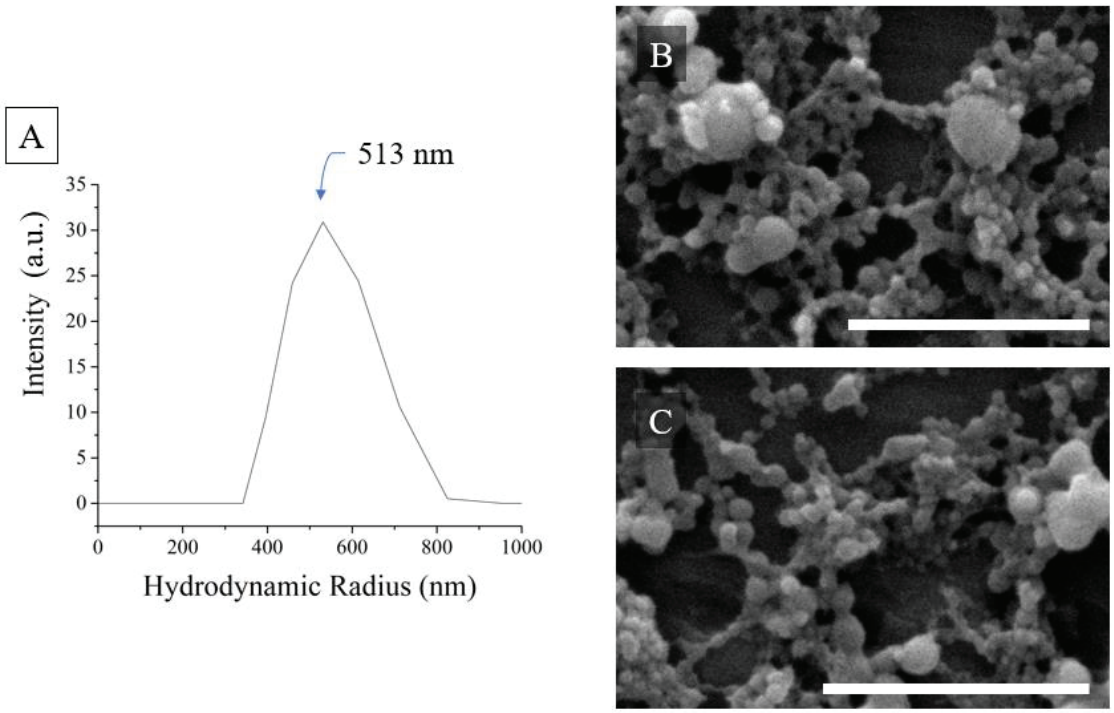

Figure 3.1. Size distribution (A) and SEM images (B and C) of BSA NPs, which were synthesized in the BmimOTf and TX-100 system (Scale bar is 1 μm).

3.1.2. Synthesis and characterization of BSA NPs in the $BmimNTf_2$ System

$BmimNTf_2$ ionic liquid was chosen as a model IL to investigate the microemulsion system of hydrophobic ionic liquids on nanoparticle formation. Microemulsions of $BmimNTf_2$ were used with two different surfactants: Tween 20 and Triton X-100/1-butanol. $BmimNTf_2$, Triton X-100/1-butanol, and water microemulsion system was already studied.[24] Ternary phase diagram of the $BmimNTf_2$/Triton X-100:BuOH/water system is shown in figure 3.2. In addition to TX-100/1-butanol consisting microemulsion, Tween 20 ternary phase diagram was obtained. Here, $BmimNTf_2$ / Tween-20 / water, ternary phase diagram, was determined in figure 3.3. Phase boundaries and sub-region boundaries were plotted as described in part 2.4.

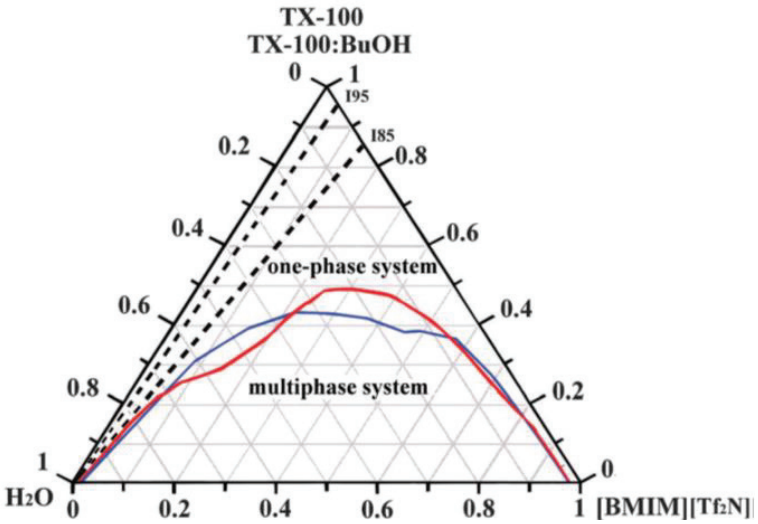

Figure 3.2. Phase diagram of aqueous $BmimNTf_2$ based ionic liquid microemulsion with (red line) and without (blue line) the presence of 1-butanol. ($BmimTf_2N$ = $BmimNTf_2$)[24]

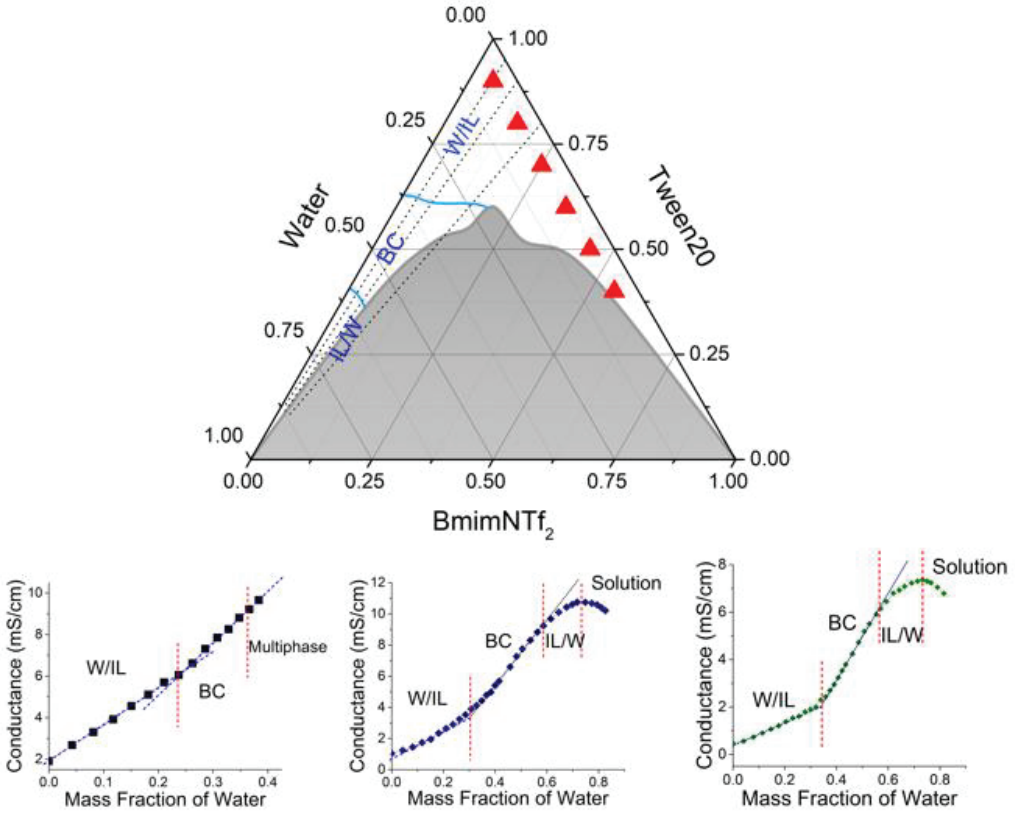

Figure 3.3. Phase diagram of $BmimNTf_2$/Tween20/water microemulsion and conductivity lines of 19:1, 9:1, and 8:2 (IL: surfactant), which were used to define the subregions of the microemulsion.

$BmimNTf_2$ / Tween 20 / water and $BmimNTf_2$ / TX-100:BuOH / water microemulsion systems have water cores in the W/IL subregion. IL and surfactant ratios were altered systematically by keeping water content constant to investigate the effects of proportions of IL and surfactant quantities in the microemulsion system on the size distribution and morphology of synthesized BSA NPs. The investigated ratios were marked as red triangles in figure 3.3.

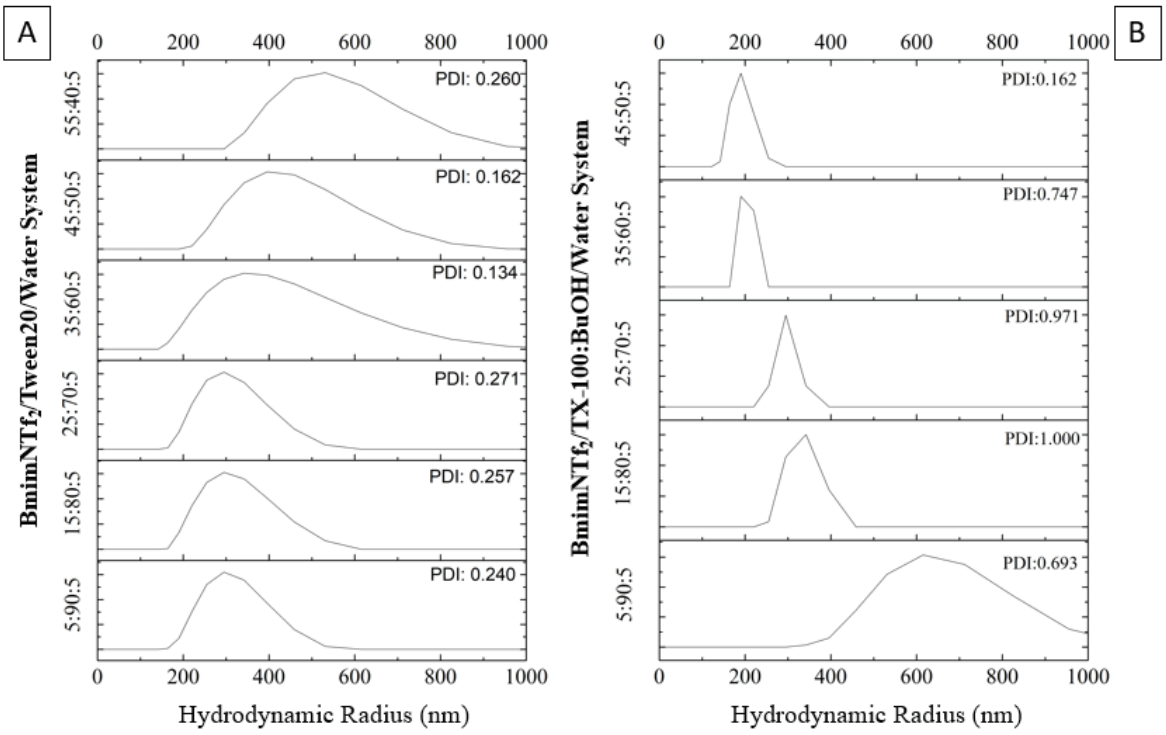

Figure 3.4. Size distributions of BSA NPs which were synthesized by $BmimNTf_2$ IL microemulsion systems in different surfactant ratios (W/IL subregion) of $BmimNTf_2$/Tween 20/water (A), and $BmimNTf_2$/TX-100:BuOH/water (B) in constant 5% (wt.%) water.

Microemulsion system regions of W/IL were investigated in constant water ratio by altering surfactant and ionic liquid amounts. BSA NP particle size distribution narrowed, and sizes of particles decreased while increasing the Tween 20 amount (Figure 3.4. (A)). Increasing Tween 20 surfactant amount stabilized the water cores in the microemulsion system, and thermodynamic stability of microemulsion increased by the same trend. While applying the high-speed homogenizer, the kinetic stability of the microemulsion also increased. In this way, smaller nanoparticles could be solidified in a

smaller core by crosslinker, and narrower size distribution could be obtained. SEM images of synthesized BSA NPs in $BmimNTf_2$/Tween 20/water and $BmimNTf_2$/TX-100:BuOH/water systems were shown in figure 3.5.

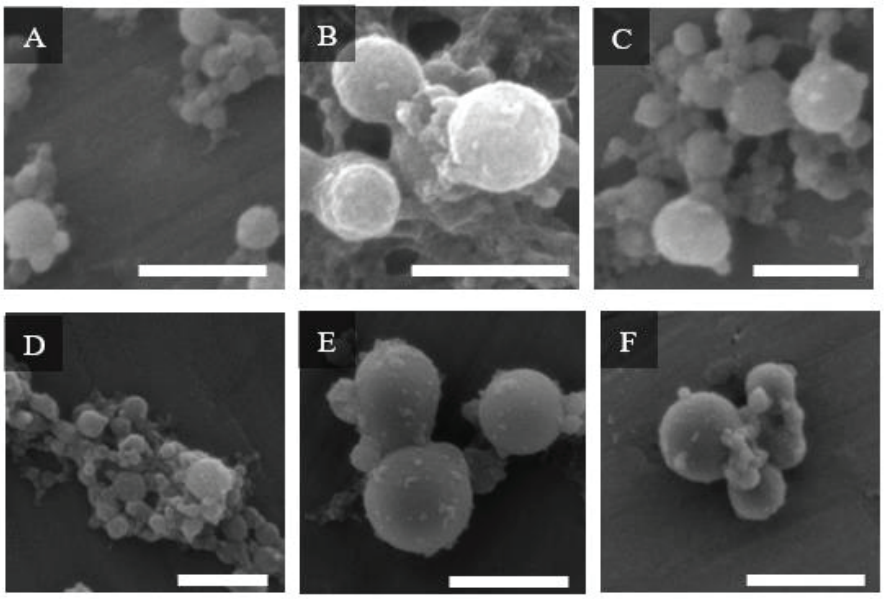

Figure 3.5. SEM images of BSA NPs synthesized in $BmimNTf_2$/Tween 20/water system in 5:90:5 (wt.%) (A), 15:80:5 (wt.%) (B), and 35:60:5 (wt.%) (C), and $BmimNTf_2$/TX-100:BuOH/water system in 5:90:5 (wt.%) (D), 15:80:5 (wt.%) (E), 25:70:5 (wt.%) (F) (Scale bar is 500 nm).

In contrast to Tween 20, Triton X-100 surfactant at high percentages caused larger particle size and nonuniform size distributions (Figure 3.4. (B)). Within the increasing TX-100 amount in microemulsion resulted in broader particle size distributions. Oxyethylene (OE) groups of TX-100 and Tween 20 surfactants interact with positively charged imidazolium ring of IL cation. $Bmim^+$ cation-π, π-π interactions, hydrogen bonding, and van der Waals forces are crucial in these interactions.[39] The hydrophilic-lipophilic balance (HLB) is used in surfactant chemistry to describe the solubility of a surfactant in water or a nonpolar phase. HLB of Tween 20 and TX-100 were reported as 16,7 and 13,5, respectively.[40,41] Depending on these values, TX-100 molecules are less hydrophilic than Tween 20 molecules. Accordingly, within the increasing amount of Tween 20, the water cores of the microemulsion system can be stabilized by the hydrophilic OE groups of Tween 20 more efficiently. The size distribution results were consistent with reported BSA NP synthesis in the hydrophobic IL $BmimPF_6$

microemulsion system.[42] Despite that, TX-100 amount in increasing trend resulted in wider nanoparticle size distribution. NTf_2^- anions have weaker interactions with $Bmim^+$ cation when compared to $BmimPF_6$ due to greater anion size, less charge density, and weaker electrostatic forces.[24] The occurred competition between H_2O molecules and TX-100 atoms forwarded to $Bmim^+$-TX-100 interactions. As a result, a decreasing interaction between ion pairs of IL has occurred, and the increase in Triton X-100 amount in the microemulsion system has resulted in a more viscous system and larger nanoparticle size distribution. Furthermore, depending on the characteristics of surfactants, BSA NP size distribution changed as a responsive trend. These results show that, with the help of the designable content of IL and surfactants, the BSA NP size and uniformity can be altered.

In the presence of butanol as a co-surfactant in the microemulsion system, TX-100 molecules interact with butanol. Thereby, the viscosity of the microemulsion decreased, and IL mobility increased.[24] Presence of co-surfactant, microemulsion system become more stable. Besides the ratio of microemulsion components, also co-surfactants and their interactions in microemulsions were investigated. Instead of 1-butanol, various alcohol types; ethanol, propanol, and hexanol were used to formulate microemulsion by direct replacement of 1-butanol in 35:60:5 ($BmimNTf_2$/TX-100:BuOH/water) microemulsion system.

Within the addition of co-surfactants, the hydrophobicity of microemulsion increased regarding the chain length of the co-surfactant for ethanol, propanol, and butanol.[43] The increasing hydrophobicity within the increasing chain length of co-surfactants may cause stricter co-surfactant-$Bmim^+$ cation interaction. However, when hexanol was used as a co-surfactant, the size and size distribution of the BSA NPs increased (Figure 3.6.). Thus, the longer chain of hexanol may interact with $Bmim^+$ cations and induce a more viscous and rigid microemulsion structure that can be the reason for larger water cores and more micron-sized particles.

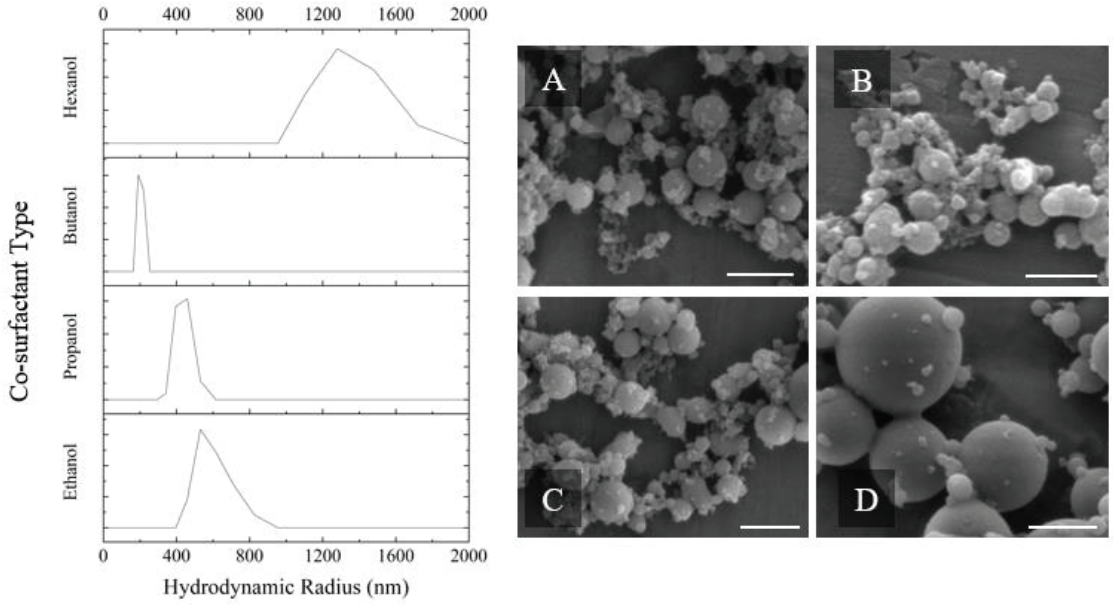

Figure 3.6. Size distributions obtained by DLS (left) and SEM images of BSA NPs (right) which were synthesized by addition of different types of co-surfactants; ethanol (A), propanol (B), butanol (C), and hexanol (D) in $BmimNTf_2$/TX-100 system. (Scale bar is 1 μm)

3.2. Drug Loading of BSA NPs

3.2.1. UV-Vis Spectrometry Analysis of Chlorambucil

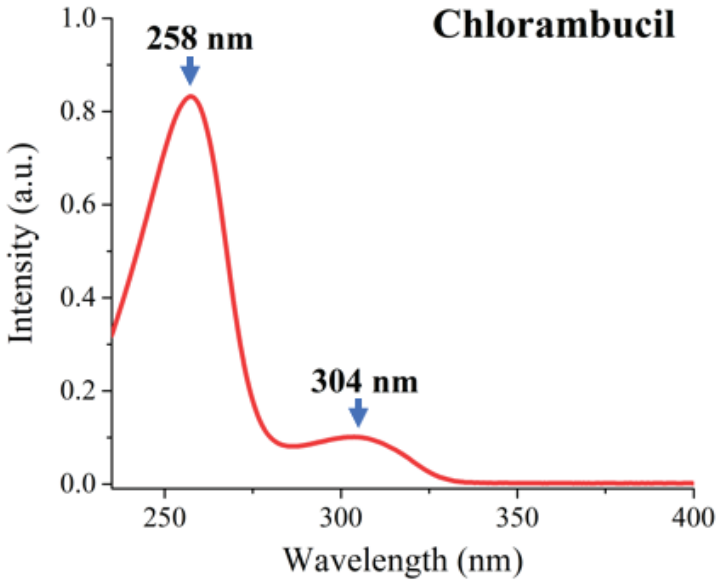

Figure 3.7. UV-Vis spectrum of 9,6 x 10^{-5} M CHL in 1% (v/v) DMSO aqueous solution.

Chlorambucil is a UV-active drug because of π-π* and n-π* electron transitions of the benzamine group of the molecule. 9,6 x 10^{-5} M chlorambucil in 1% (v/v) DMSO:water solution sample was measured by UV-Vis spectrometer. The maximum absorbance peaks (λ_{max}) were found at 258 nm and 304 nm (Figure 3.7.).

Various concentrations of CHL in 1% (v/v) DMSO-water solution were measured by UV-Vis spectrophotometer (Figure 3.8.). According to the results, CHL was not completely dissolved over the 3,2 x 10^{-4} M in that solvent combination.

The amount of loaded chlorambucil on the BSA NPs was determined by measuring the supernatant by UV-Vis spectroscopy. The drug loading was calculated by subtracting the CHL amount in the supernatant from the initial CHL. Thus, the loaded CHL amount in the BSA NPs pellet was determined by formulas 1 & 2 in part 2.3.4.

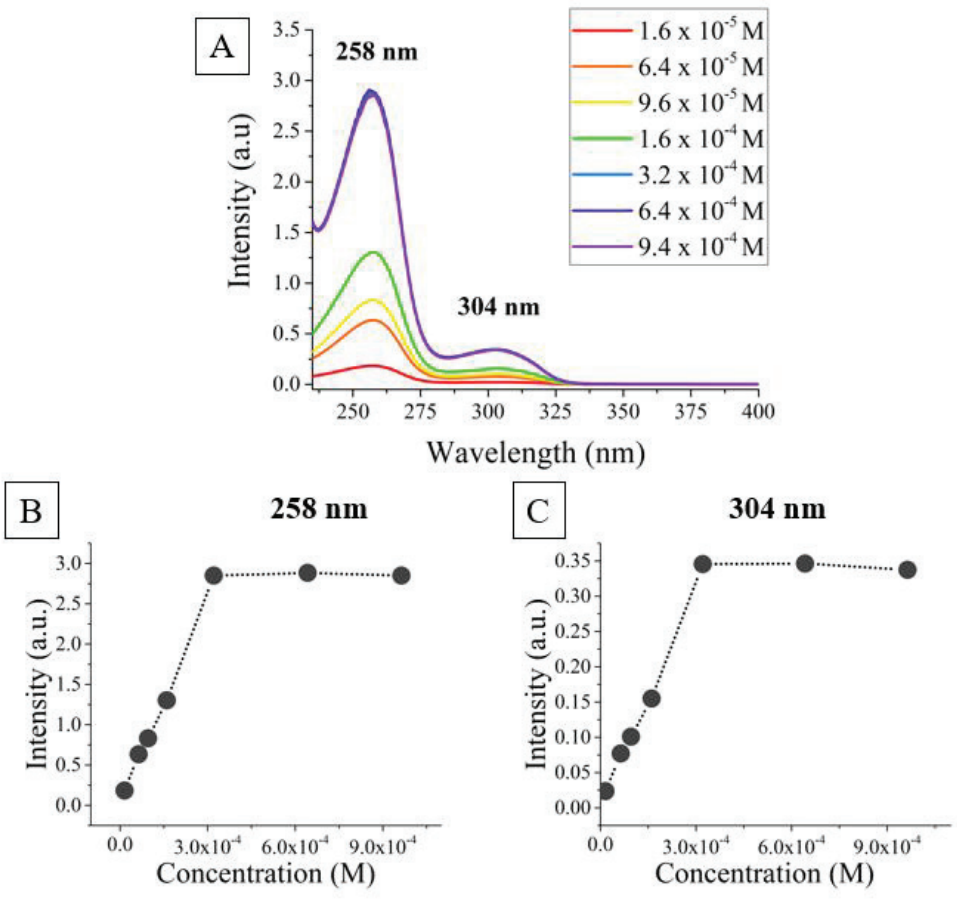

Figure 3.8. (A) UV-Vis spectra of various concentrations of CHL in 1% (v/v) DMSO aqueous solution. (B) Absorbance intensities of CHL in various concentrations at 258 nm. (C) Absorbance intensities of CHL in various concentrations at 304 nm.

3.2.2. Characterization of CHL Loaded BSA NPs Synthesized in $BmimBF_4$/TX-100/Water System

Drug loading experiments were conducted in two methods. In the first method, CHL was introduced during the synthesis of BSA NPs (Parts 2.3.2), and in the second method, CLH and synthesized NPs were incubated (Part 2.3.4).

3.2.2.1. CHL Loaded BSA NP Synthesis by CHL Loaded BSA in $BmimBF_4$/TX-100/Water System

$BmimBF_4$/TX-100/1-butanol 1% (v/v) DMSO and 8% water mixture was used as a blank solution in the UV-Vis analysis (Figure 3.9.). Although chlorambucil has a sharper signal at 258 nm, the mixture of $BmimBF_4$/TX-100/1-butanol 1% (v/v) DMSO and 8% water UV-Vis spectrum covers the region of the 200-300 nm wavelengths. Therefore, the second λ_{max} of the absorption at 304 nm was used to evaluate CHL quantity.

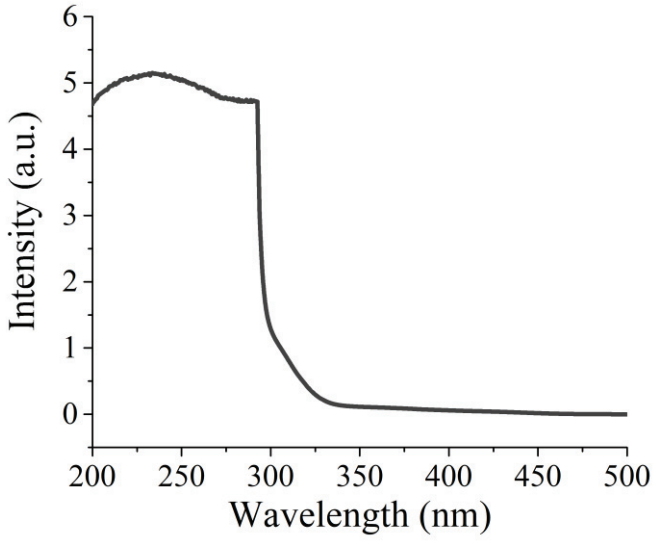

Figure 3.9. UV-Vis spectrum of $BmimBF_4$/TX-100 system (Blank sample).

Particular amounts of CHL including $BmimBF_4$/TX-100/1-butanol 1% (v/v) DMSO and 8% water mixtures were prepared, and reference calibration curve was plotted

by the intensities at 304 nm. $BmimBF_4$/TX-100/1-butanol 1% (v/v) DMSO and 8% water mixture was used as blank solution (Figure 3.10.).

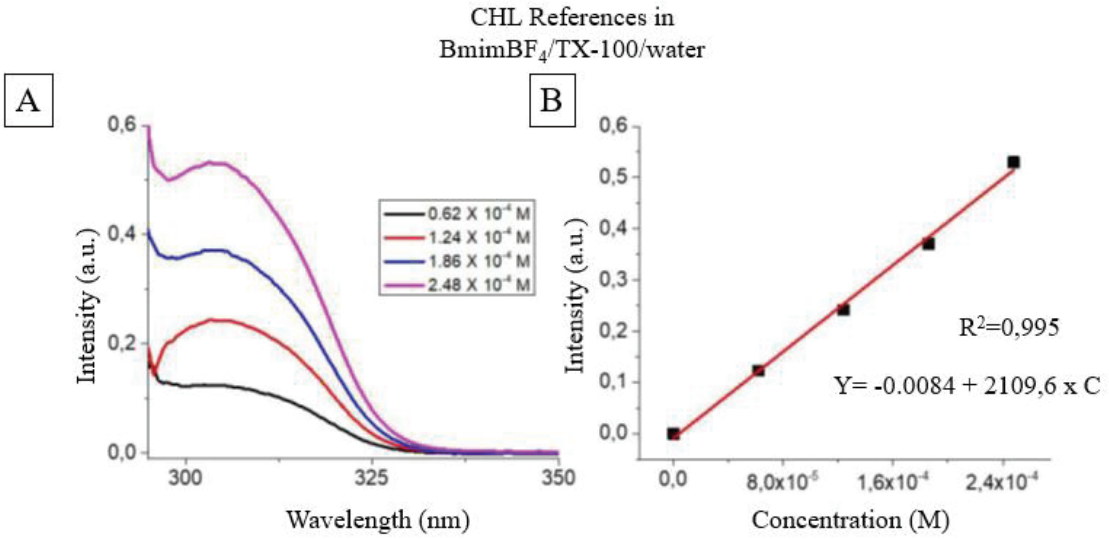

Figure 3.10. (A) UV-Vis spectra of the 0.62 x 10^{-4} M, 1.24 x 10^{-4} M, 1.86 x 10^{-4} M, and 2.48 x 10^{-4} M CHL including $BmimBF_4$/TX-100/1-butanol 1% (v/v) DMSO and 8% water mixtures. (B) The obtained calibration curve for CHL at 304 nm.

As described in part 2.3.2, 12 mg BSA is mixed with various amounts of CHL (BSA:CHL ratios were 1:1, 1:2, 1:3, and 1:4) and introduced to the system. BSA concentration on the final mixture was 0.62 x10^{-4} M, and CHL concentrations were 0.62 x 10^{-4} M, 1.24 x 10^{-4} M, 1.86 x 10^{-4} M, and 2.48 x 10^{-4} M. After NP synthesis, the BSA NP pellet was flocculated by centrifuge and then decanted supernatant was analyzed to determine the free unbound CHL amount. The UV-Vis spectra of the supernatants are shown in figure 3.11. These spectra were obtained by removing the spectrum of CHL-free $BmimBF_4$/TX-100/1-butanol 1% (v/v) DMSO and 8% water mixture from the UV-Vis spectrum of CHL including supernatants. The higher ratios of CHL were not investigated because of the solubility limit of CHL in 1% DMSO (v/v) water solution and the denaturation risk of the BSA. In the literature, it has been shown that, maximum two chlorambucil molecules bound to BSA protein.[31]

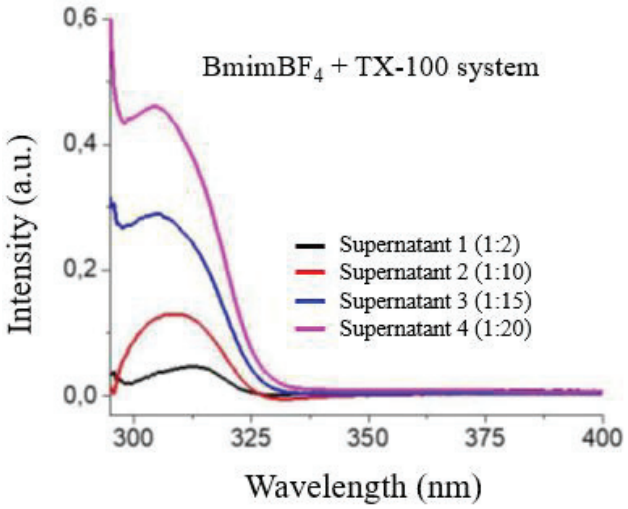

Figure 3.11. UV-Vis spectra of free-CHL remaining in the supernatants obtained by flocculating CHL loaded BSA NPs synthesized by $BmimBF_4$/TX-100: BuOH/water system.

Drug entrapment efficiencies and drug loading capacities of synthesized BSA NPs were calculated using formulas 1 and 2 in part 2.3.4 (Figure 3.12.). While BSA: CHL mol ratio 1:1, drug entrapment efficiency was found 67%. The higher CHL ratios, 1:2, 1:3, and 1:4, were 48%, 25%, and 11%, respectively. BSA NP synthesis yielded 71%. Drug loading capacities were calculated as 0,44% (1:1), 0.64% (1:2), 0.49% (1:3) and 0.29% (1:4).

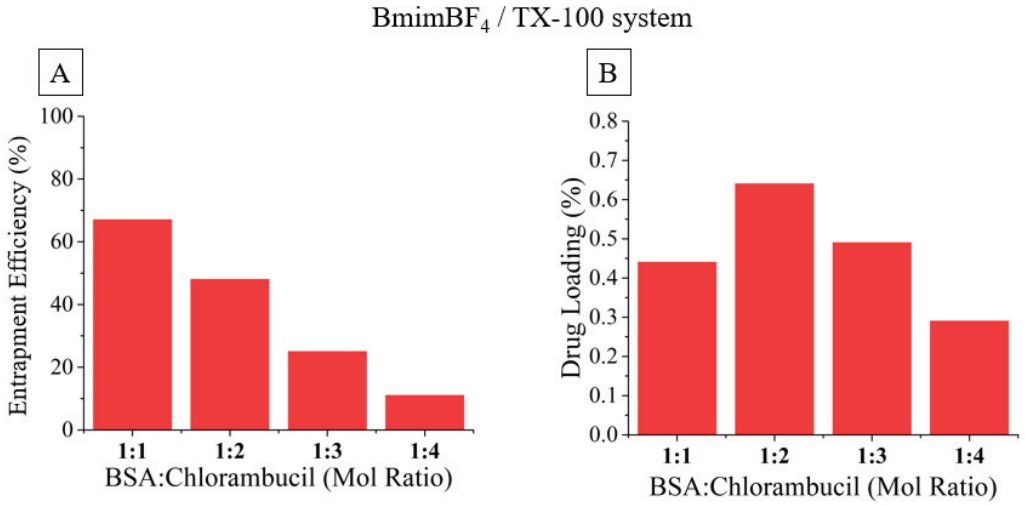

Figure 3.12. CHL entrapment efficiencies (A) and loading capacities (B) of BSA NPs obtained by $BmimBF_4$/TX-100: BuOH/water system.

3.2.2.2. CHL Loading to BSA NPs Synthesized in $BmimBF_4$/TX-100/Water system

BSA NPs were obtained as described in part 2.2.1, and CHL was loaded to the particles as described in part 2.3.4. After purification steps, 4,26 mg BSA NPs were dispersed in 1 mL ultrapure water with the help of vortex and sonic bath. Determined amounts CHL solutions were prepared as to be 1:2, 1:10, 1:15, 1:20 and 1:25 (BSA:CHL) ratio by dissolving in 1 mL 30% (v/v) DMSO aqueous solvent. Two solutions were mixed, and BSA NPs and CHL solutions were incubated for 24 h under continuous shaking. (The final concentration of BSA: 2.4 x 10^{-5} M, final DMSO content: 15% (v/v)). After the incubation period, the BSA NPs were separated from the suspension by centrifugation, and the supernatant was analyzed to determine unbound CHL quantity by UV-Vis spectrometer in the range of 200-500 nm.

Determined concentrations of CHL in 15% (v/v) DMSO and water solutions were prepared, and these solutions were used to plot the calibration curve at 304 nm. The result shows that 8.2 x10^{-4} M was out of the trend due to poor CHL solubility. Thus, 6.4 x 10^{-5} M CHL concentration was accepted as the upper limit for the calibration (Figure 3.13.).

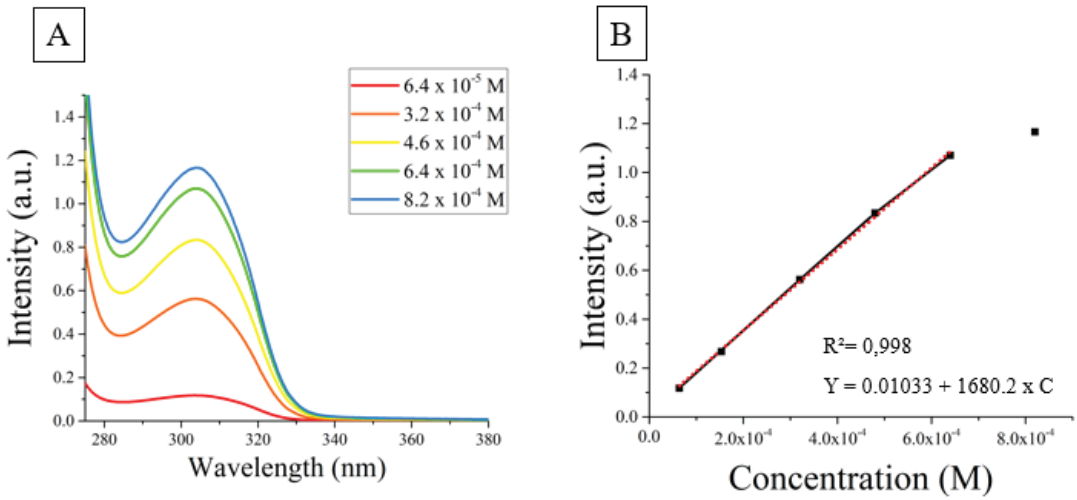

Figure 3.13. (A) UV-Vis spectra of 6.4 x 10^{-5} M, 3.2 x 10^{-4} M, 4.8 x 10^{-4} M, 6.4 x 10^{-4} M, and 8.2 x 10^{-4} M CHL including 15% (v/v) DMSO-Water solutions. (B) The calibration curve was obtained from absorbance signal of CHL at 304 nm.

CHL entrapment efficiency and loading capacities were calculated with the help of the calibration curve and formulas 1 and 2 in part 2.3.4. CHL entrapment efficiencies of BSA NPs were found 73% for 1:2 BSA:CHL ratio, and ≈78% for the rest. The drug loading capacities for 1:2, 1:10, 1:15, 1:20 and 1:25 were found as 0.7%, 3.6%, 5.3%, 6,5% and 8.1%, respectively (Figure 3.14.).

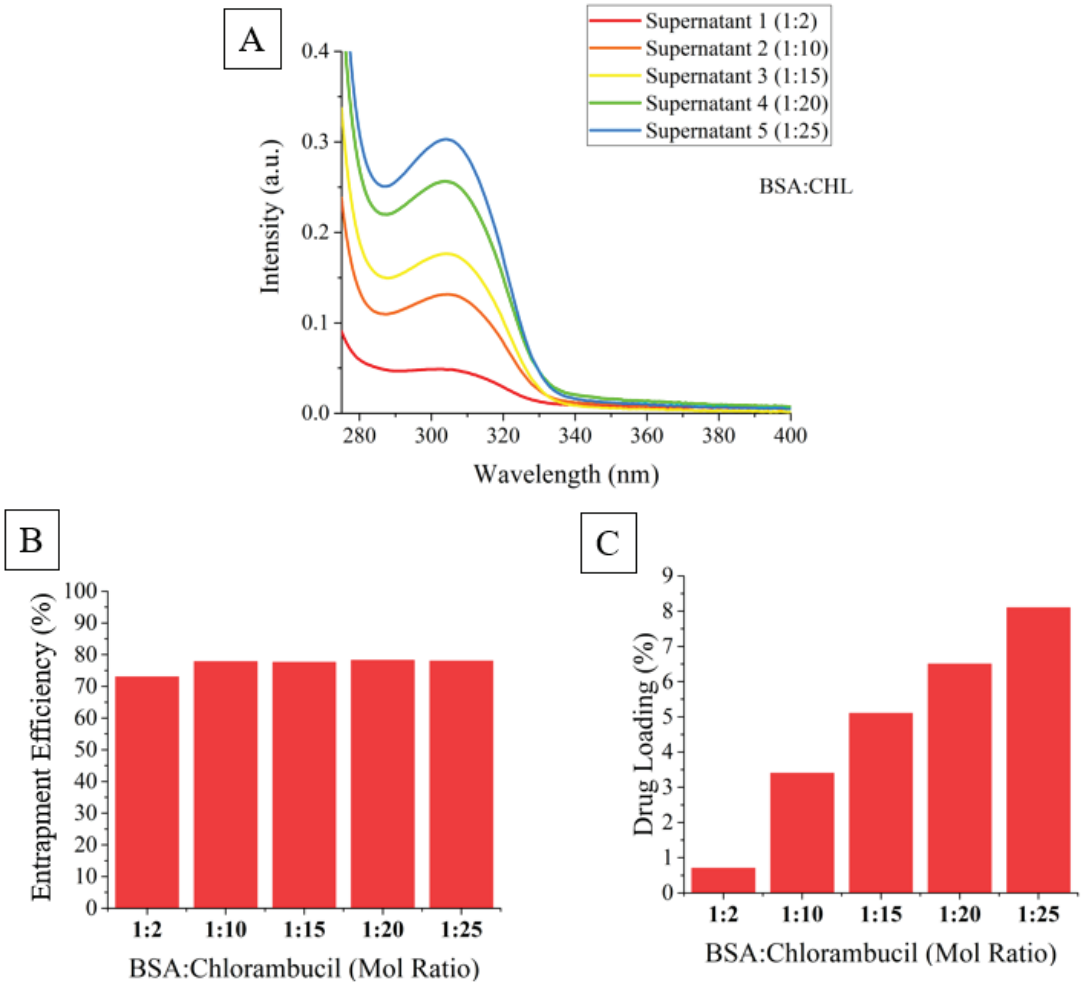

Figure 3.14. (A) UV-Vis spectra of the supernatants obtained by centrifugation of CHL incubated BSA NPs synthesized in $BmimBF_4$/TX-100:BuOH/water system. (B) Drug entrapment efficiencies and (C) drug loading capacities of BSA NPs.

3.2.3. Characterization of CHL Loaded BSA NPs Synthesized in $BmimPF_6$/TX-100/Water System

Drug loading experiments were conducted in two methods. In the first method, CHL was introduced during the synthesis of BSA NPs (Part 2.3.3), and in the second method, CLH and synthesized NPs were incubated (Part 2.3.4).

3.2.3.1. CHL Loaded BSA NP Synthesis by CHL Loaded BSA in $BmimPF_6$/TX-100/Water System

The BSA-CHL solution was prepared as described in part 2.3.1. Determined amounts of CHL were incubated with BSA, and the DMSO content was kept constant as 2.8% (v/v) at each mol rate of BSA:CHL (1:1, 1:2, 1:3 and 1:4) in incubation solvent and 1% (v/v) in the final mixture. 2x methanol (4 mL) was introduced to the suspension to precipitate the BSA NPs, and after centrifugation, supernatants were saved for UV-Vis spectrometry analysis to detect unbound CHL quantity. Added MeOH was also included in the blank $BmimPF_6$/TX-100/water (45:50:5 (wt.%)) 21.4 µL DMSO mixture (Figure 3.15.).

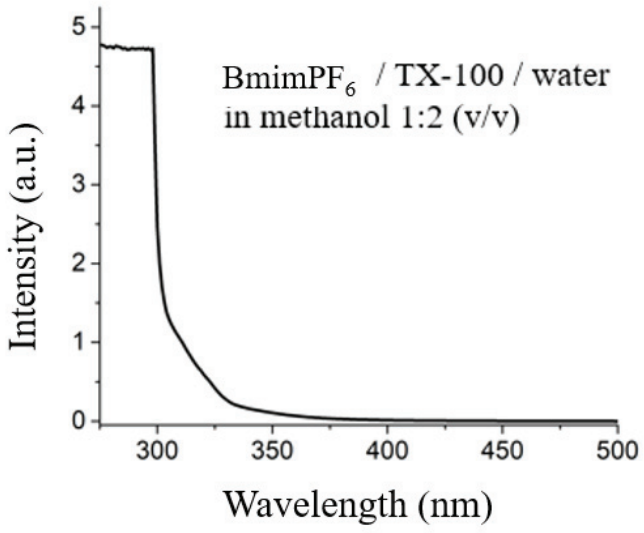

Figure 3.15. UV-Vis Spectrum of $BmimPF_6$/TX-100/water (45:50:5 wt.%) 1% (v/v) DMSO. The mixture was measured in 1:2 (v/v) MeOH (Blank solution curve).

As a reference calibration curve, determined amounts of CHL including $BmimPF_6$/TX-100/water and 1:2 (v/v) MeOH mixtures were prepared, and UV-Vis spectra were obtained by removing the spectrum of blank solution. The absorbance intensities at 304 nm were used to plot the calibration curve of CHL in the concentrations of 2.2 x 10^{-5} M, 4.4 x 10^{-5} M, 6.6 x 10^{-5} M, and 8.8 x 10^{-5} M (Figure 3.16.).

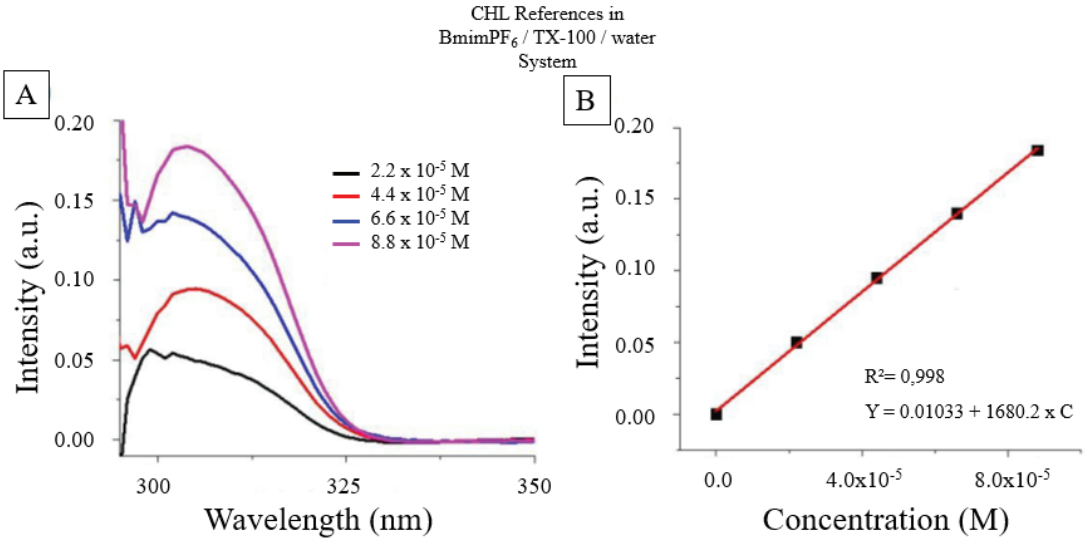

Figure 3.16. (A) UV-Vis spectra of 2.2 x 10^{-5} M, 4.4 x 10^{-5} M, 6.6 x 10^{-5} M, and 8.8 x 10^{-5} M CHL including $BmimPF_6$/TX-100/water and 1:2 (v/v) MeOH mixtures which were obtained by removing the UV-Vis Spectrum of blank solution. (B) The obtained calibration curve for CHL at 304 nm.

As described in part 2.3.3, the supernatant was analyzed in the UV-vis spectrometer. With the help of this analysis, CHL entrapment efficiencies and loading capacities were calculated with the help of the calibration curve and formulas 1 and 2 in part 2.3.4. CHL entrapment efficiencies of BSA NPs were found 25% for 1:1 BSA:CHL ratio and 23% for 1:2. For the 1:3 ratio reduced to 17% and reached the minimum, 12% for the 1:4. The drug loading capacities were calculated by regarding of 72% formation yield of BSA NP on that system, and were found as 0,16%, 0,30%, 0,35% and 0,30% for 1:1, 1:2, 1:3 and 1:4 ratios, respectively (Figure 3.17.).

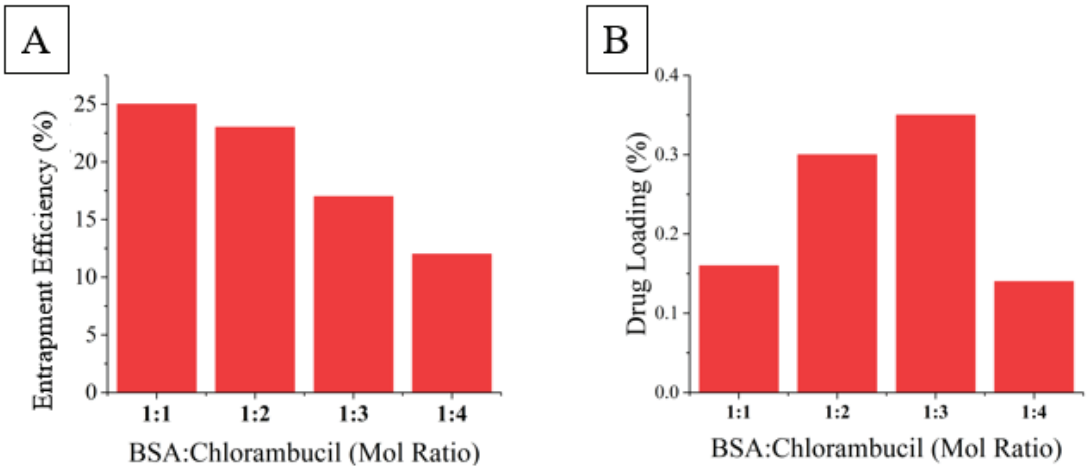

Figure 3.17. CHL entrapment efficiencies (A) and loading capacities (B) of BSA NPs obtained by CHL-BSA incubation in 1:1, 1:2, 1:3, and 1:4 ratios and synthesized in $BmimPF_6$/TX-100:BuOH/water system.

3.2.3.2. CHL Loading to BSA NPs Synthesized in $BmimPF_6$/TX-100/Water System

BSA NPs were synthesized, and the obtained BSA NPs were incubated with CHL (Part 2.3.4). Incubated BSA NPs were separated by centrifugation and were used for the detection of unbound CHL quantity. Entrapment efficiencies and drug loading capacities were calculated using formulas 1 and 2 in part 2.3.4. The calibration curve of CHL and absorbance signals of supernatants at 304 nm were used to assess the CHL amount in the supernatants.

Entrapment efficiencies of BSA NPs were found as 68%, 80%, 72% and 72% for the 1:2, 1:10, 1:15 and 1:25 of the BSA:CHL ratios, respectively (Figure 3.18.). Loading capacities were found as 0.06% for 1:2 (BSA:CHL), 3.8% for 1:10, 5.2% for 1:15 and 7.9% for 1:25.

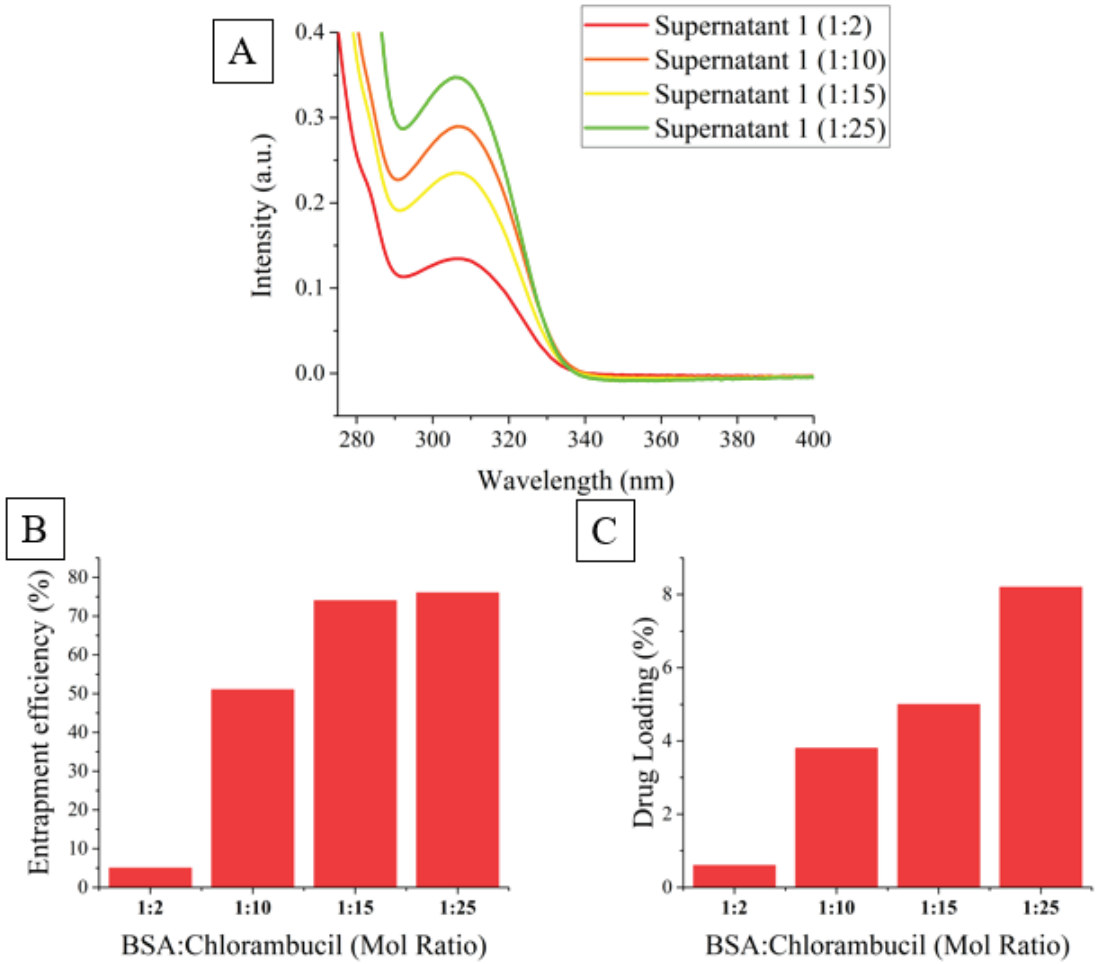

Figure 3.18. UV-Vis spectra of the supernatants obtained by centrifugation of CHL incubated BSA NPs synthesized in $BmimPF_6$/TX-100/water system. (B) CHL entrapment efficiencies and (C) drug loading capacities of BSA NPs.

3.2.4. Characterization of CHL Loaded BSA NPs Synthesized in BmimOTf/TX-100/Water System

The same two methods were applied for BSA NPs in BmimOTf/TX-100/water system. The experiments were conducted as described in part 2.3.2. However, due to the broader UV-Vis absorption range of BmimOTf IL, the determination of the amount of CHL method was incompatible with the UV-Vis spectroscopy analysis. UV-Vis spectrum of BmimOTf/TX-100/water (Figure 3.19.) clearly shows that the absorption signal of CHL is undetectable in the existence of the BmimOTf.

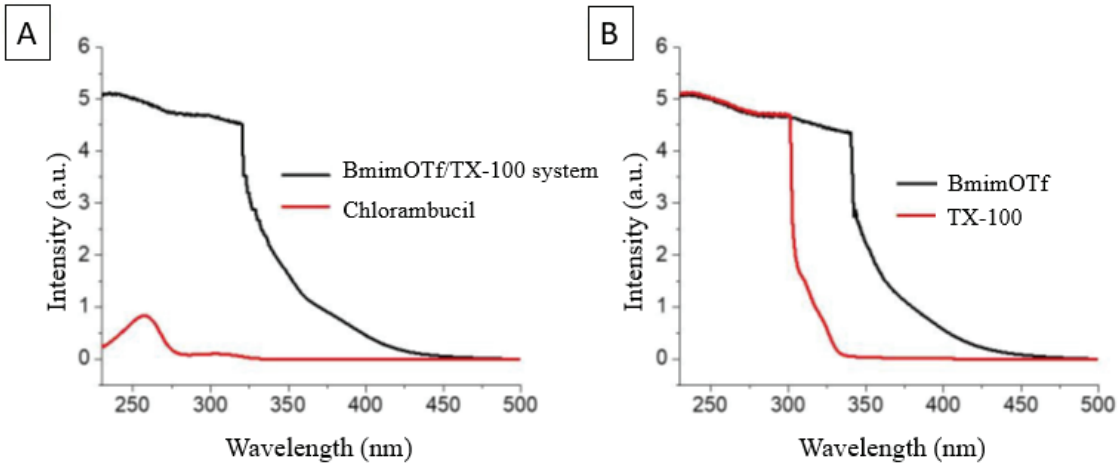

Figure 3.19. (A) UV-Vis spectra of the mixture of BmimOTf and TX-100 (black line) and the absorbance signal of desired CHL (red line). (B) UV-Vis spectrum of BmimOTf (black line) and surfactant TX-100 (red line).

3.2.4.1. CHL Loading to BSA NPs Synthesized in BmimOTf/TX-100/Water system

BSA NPs were synthesized like described in part 2.2.1, and CHL was loaded to the BSA NPs (Part 2.3.4) by incubation with 1:2, 1:10, 1:15, and 1:25 (BSA:CHL mol ratio) CHL. The calibration curve of CHL and the absorbance signals of supernatants at 304 nm were used to estimate the CHL amounts in the supernatants. Entrapment efficiencies and drug loading capacities were calculated by formulas 1 and 2 in part 2.3.4.

Entrapment efficiencies were found as 9.2% for 1:2, 17.7% for 1:10, 26.1% for 1:15, 57.8% for 1:25 and, drug loading capacities were found as 0.08%, 0.8%, 1.75%, 6.2% for 1:2, 1:10, 1:15 and 1:25 BSA:CHL mol ratios, respectively (Figure 3.20.).

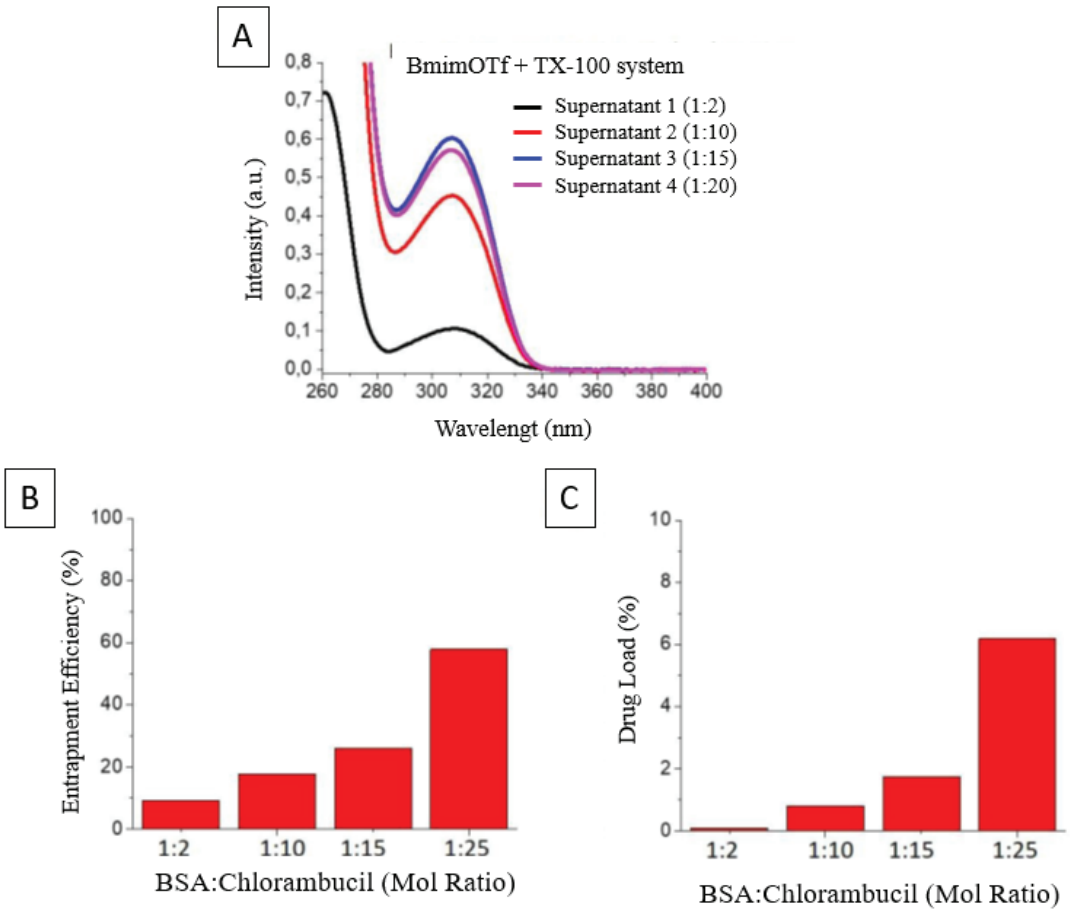

Figure 3.20. (A) UV-Vis spectra of the supernatants obtained by centrifugation of CHL incubated BSA NPs synthesized in BmimOTf/TX-100/water system. (B) CHL entrapment efficiencies and (C) drug loading capacities of BSA NPs.

3.2.5. Characterization of CHL Loaded BSA NPs Synthesized in $BmimNTf_2$/TX-100/Water System

Drug loading experiments were conducted in two methods. In the first method, CHL was introduced during the synthesis of BSA NPs (Part 2.3.3), and in the second method, CLH and synthesized NPs were incubated (Part 2.3.4).

3.2.5.1. BSA NP Synthesis by CHL Loaded BSA in $BmimNTf_2$/TX-100/Water System

The BSA-CHL solution was prepared as described in part 2.3.1. Determined amounts of CHL were incubated with BSA, and the DMSO content was kept constant as 2.6% (v/v) at each mol rate of BSA:CHL (1:1, 1:2, 1:3 and 1:4) in incubation solvent and 1% (v/v) in the final mixture. 2x methanol (5.2 mL) was introduced to the suspension to precipitate the BSA NPs, and after centrifugation, supernatants were saved for UV-Vis spectrometry analysis to detect unbound CHL quantity. Added MeOH was also included in the $BmimNTf_2$/TX-100/water (35:60:5 wt.%) 26 µL DMSO mixture (Figure 3.21.).

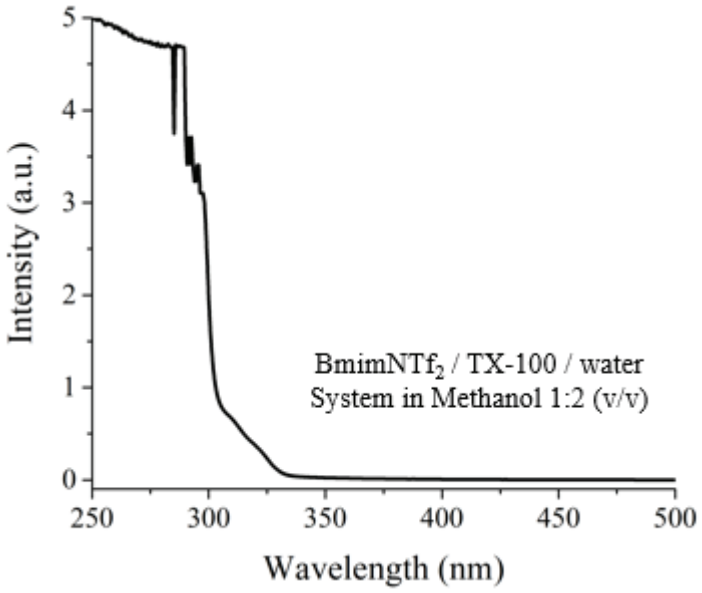

Figure 3.21. UV-Vis Spectrum of $BmimNTf_2$/TX-100/water (35:60:5 wt.%) 1% (v/v) DMSO. The mixture was measured in 1:2 (v/v) MeOH. (Blank solution curve)

As a reference calibration curve, determined amounts of CHL including $BmimNTf_2$/TX-100/water and 1:2 (v/v) MeOH mixtures were prepared, and UV-Vis spectra were obtained by removing the spectrum of blank solution. The absorbance intensities at 304 nm were used to plot the calibration curve of CHL in the concentrations of 0.25×10^{-4} M, 0.50×10^{-4} M, 0.75×10^{-4} M, and 1.00×10^{-4} M (Figure 3.22.).

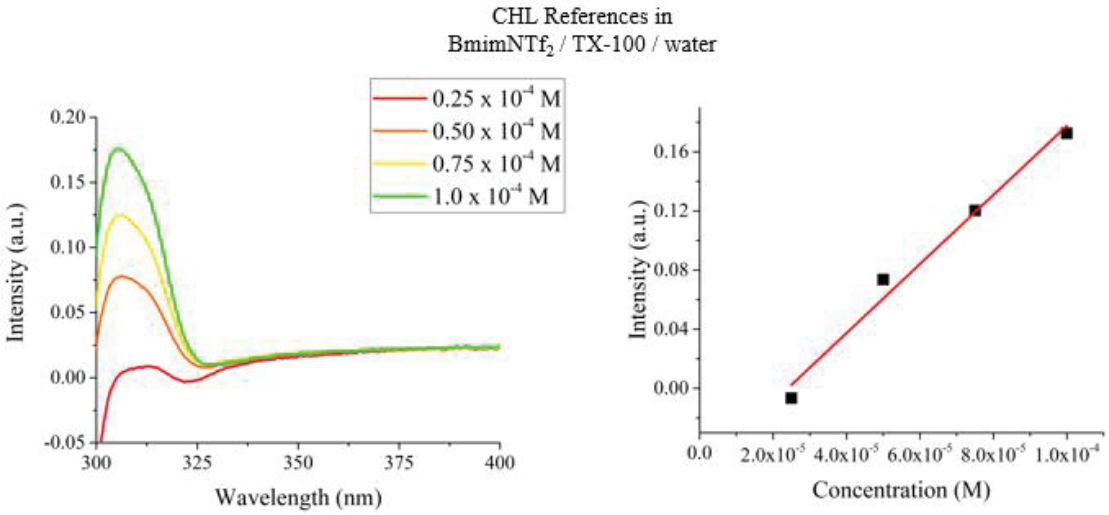

Figure 3.22. UV-Vis spectrum of 0.25 x 10^{-4} M, 0.50 x 10^{-4} M, 0.75 x 10^{-4} M and 1.00 x 10^{-4} M CHL including $BmimNTf_2$/TX-100/water and 1:2 (v/v) MeOH mixtures which were obtained by removing the UV-Vis Spectrum of blank solution (right). The calibration curve was obtained from the absorbance signal of CHL at 304 nm (left).

As described in part 2.3.4, the supernatant was analyzed by the UV-vis spectrometer. Absorbance intensities of the samples at 304 nm were used to determine drug amounts. CHL entrapment efficiencies and loading capacities were calculated with the help of the calibration curve and formulas 1 and 2 in part 2.3.4. CHL entrapment efficiencies of BSA NPs were found 0% for 1:1 BSA:CHL ratio, and 9.5% for 1:2, 28.9% for 1:3 and 19.2 for 1:4 (Figure 3.23. B). The drug loading capacities were calculated by regarding of 71% formation yield of BSA NP on that system and were found as 0%, 0,13%, 0,57% and 0,50% for 1:1, 1:2, 1:3 and 1:4 ratios, respectively (Figure 3.23. C).

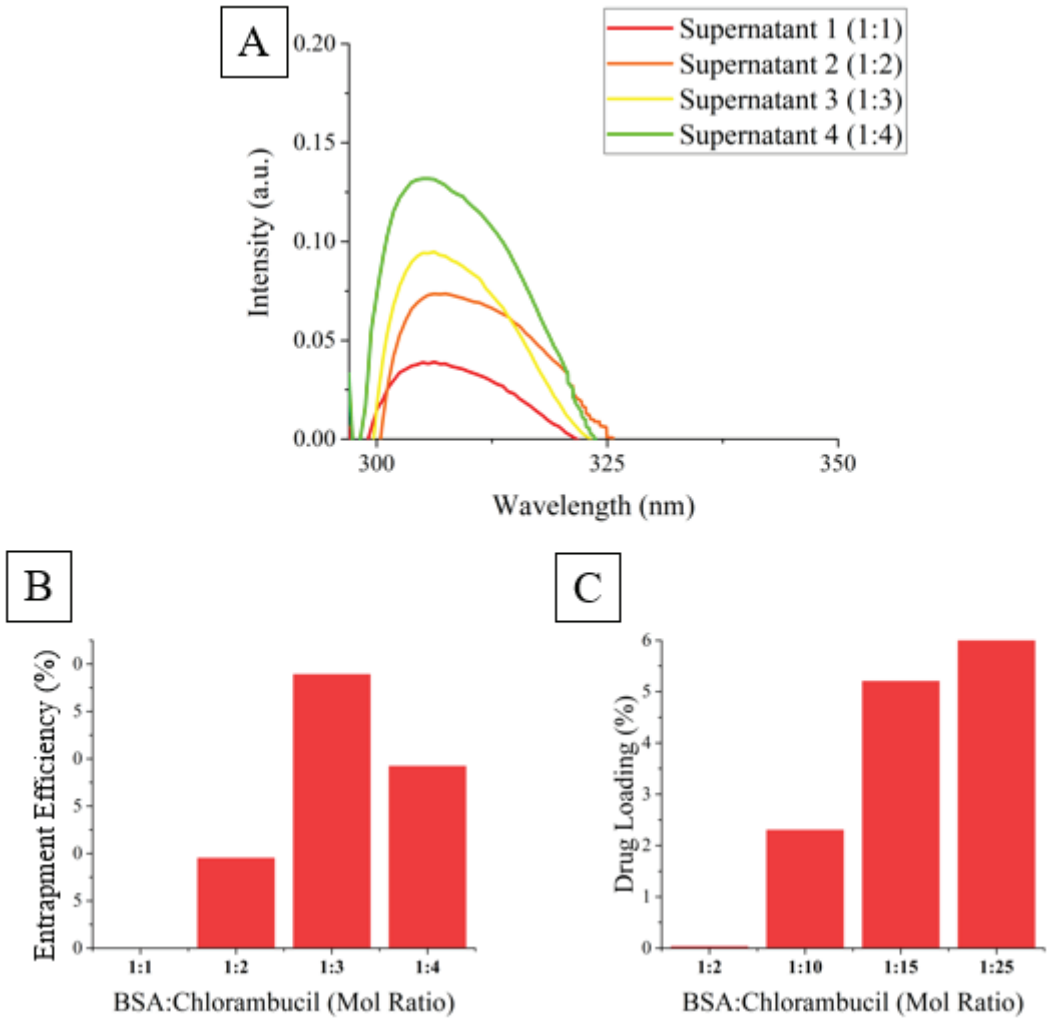

Figure 3.23. (A) UV-Vis spectra of the supernatants were obtained by centrifugation of CHL incubated BSA NPs synthesized by $BmimNTf_2$/TX-100/water system. (B) CHL entrapment efficiencies and (C) drug loading capacities of BSA NPs.

3.2.5.2. CHL Loading to BSA NPs Synthesized in $BmimNTf_2$/TX-100/Water system

BSA NPs were synthesized, and the obtained BSA NPs were incubated with CHL (Part 2.3.4). Incubated BSA NPs were separated by centrifugation and were used for assessment of unbound CHL quantity. Entrapment efficiencies and drug loading capacities were calculated by the formula 1 and 2 in part 2.3.4. The calibration curve of CHL and absorbance signal of supernatants (Figure 3.24. (A)) at 304 nm were used to estimate the CHL amount in the supernatants.

Entrapment efficiencies of BSA NPs were found as 5%, 51%, 74% and 76% for the 1:2, 1:10, 1:15 and 1:25 of the BSA:CHL ratios (Figure 3.24.). Loading capacities were found as 0.03% for 1:2 (BSA:CHL), 2.3% for 1:10, 5.2% for 1:15 and 8.4% for 1:25.

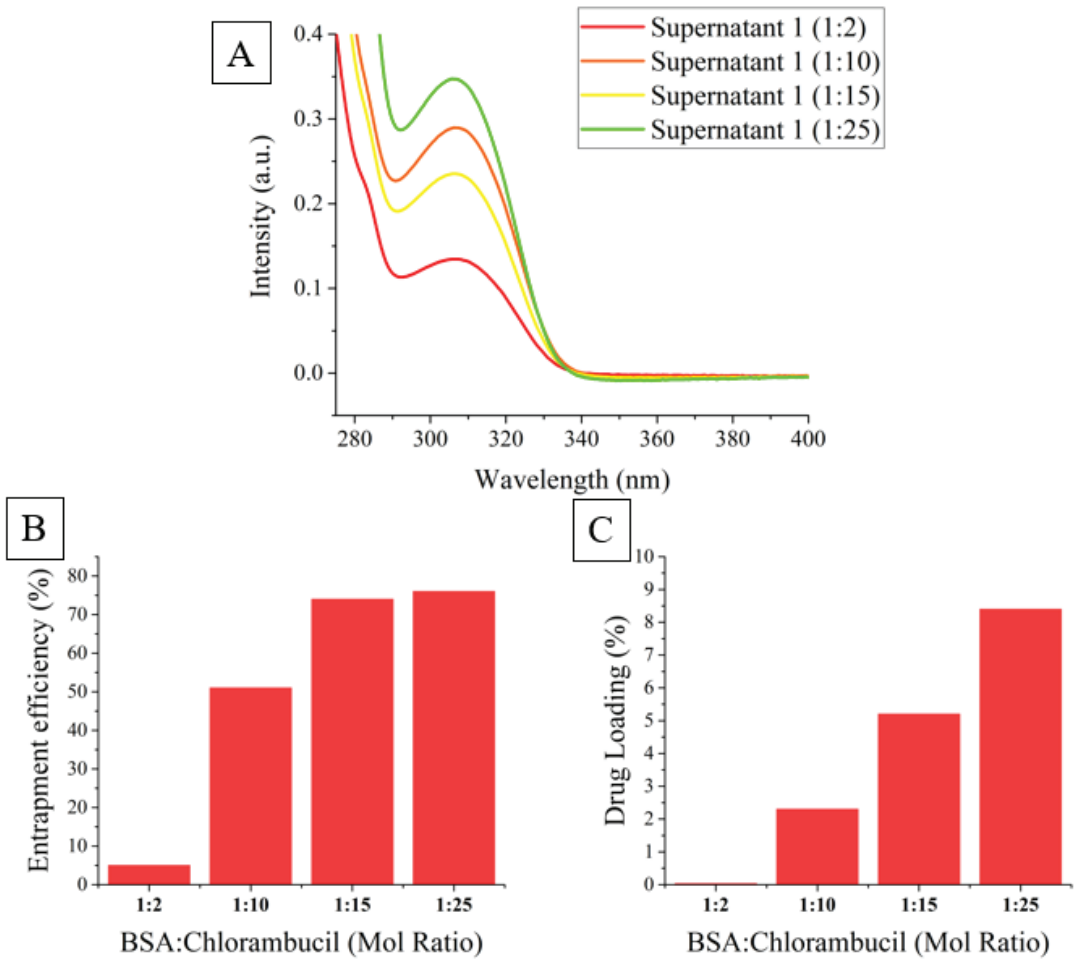

Figure 3.24. UV-Vis spectra of the supernatants were obtained by centrifugation of CHL incubated BSA NPs synthesized in BmimNTf$_2$/TX-100/water system. (B) CHL entrapment efficiencies and (C) drug loading capacities of BSA NPs.

The drug loading capacities and entrapment efficiencies of the BSA NPs synthesized in four types of IL systems were schematized in figure 3.25. as a summary.

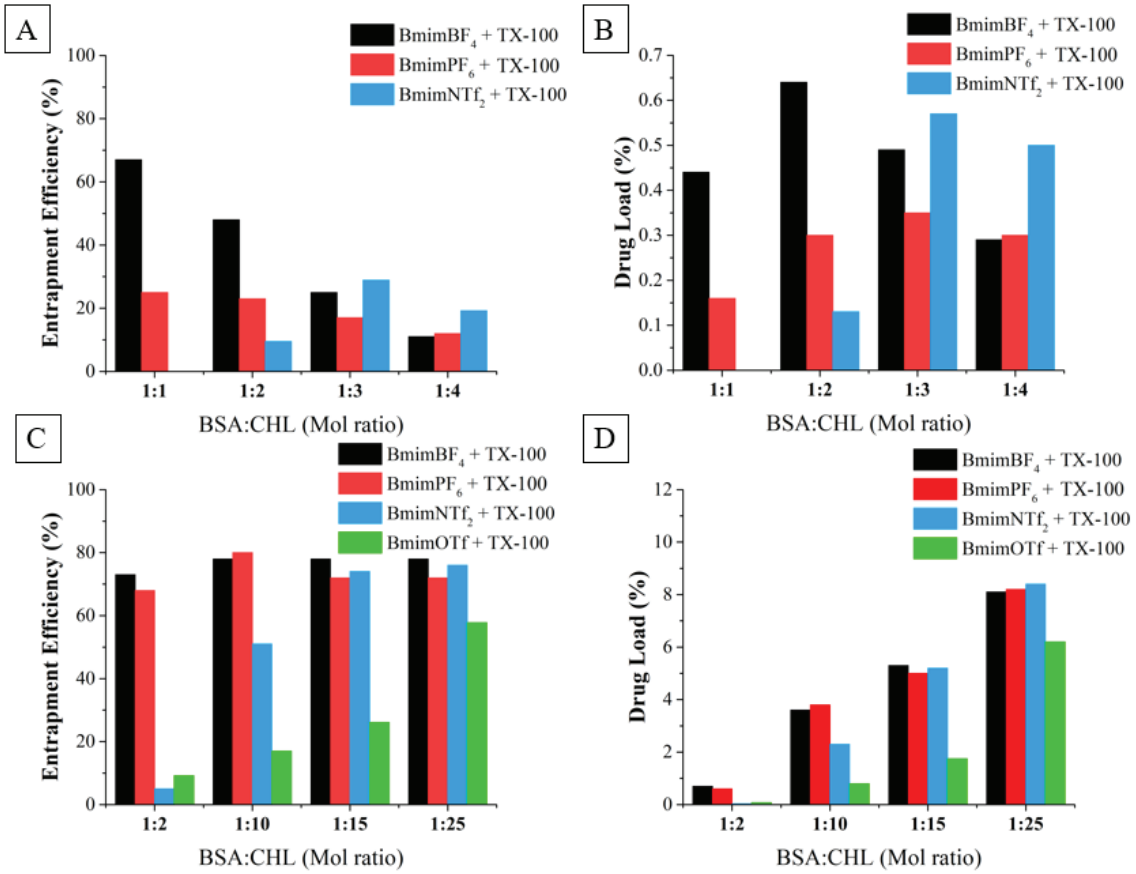

Figure 3.25. Entrapment efficiencies (A) and drug loading capacities (B) of BSA NPs which were synthesized in different IL systems ($BmimBF_4$: black, $BmimPF_6$: red, BmimOTf: green, and $BmimNTf_2$: blue columns.) and were obtained from BSA-CHL incubation (1:1, 1:2, 1:3, 1:4 BSA:CHL mol ratio). Entrapment efficiencies (C) and drug loading capacities (D) of BSA NPs incubation with CHL after synthesis (1:2, 1:10, 1:15, 1:25 are BSA:CHL mol ratio).

3.3. Drug Releasing Experiments

3.3.1. Drug Releasing of BSA NPs

Drug release investigations were done as described in part 2.3.5. In the part of drug loading 3.2, and the most efficient drug loading capacities were found at 1:25 (BSA:CHL) mol ratio of drug loaded BSA NPs after the synthesis. All drug releasing experiments were conducted in the phosphate buffer medium and BSA NP trapped dialysis tube. Firstly, drug loaded NP suspension was placed in a dialysis tube and, in the

determined time periods, samples were taken from the PB and analyzed by UV-Vis spectrometry. The released amounts were obtained from the calibration curve of chlorambucil (Y=0.0251 + 0.9789 x C, R^2=0.9999).

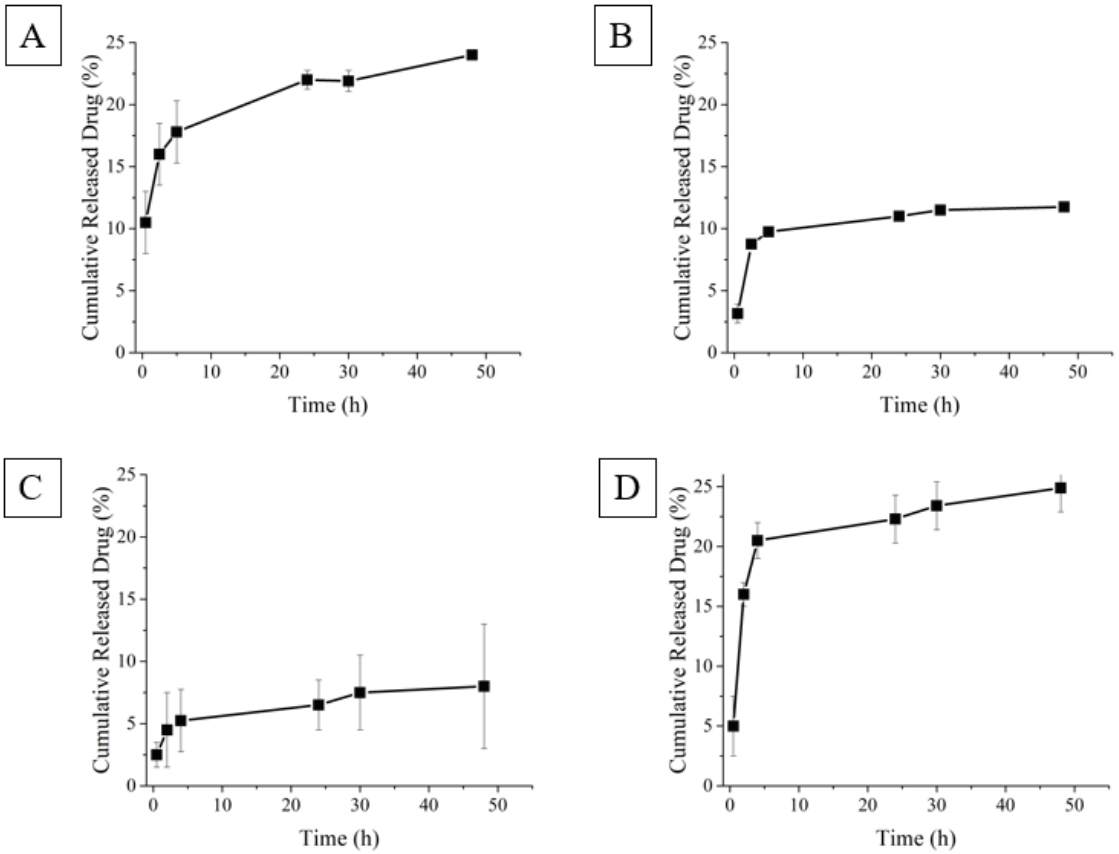

Figure 3.26. Cumulative percentages of CHL released from the BSA NPs which were obtained in (A) $BmimBF_4$/TX-100/water, (B) $BmimPF_6$/TX-100/water, (C) $BmimNTf_2$/TX-100/water, and (D) BmimOTf/TX-100/water systems in 0.1 M PB (pH=7.4, 37 °C) medium.

Cumulative releasing percentages of CHL, which were released from the BSA NP, were investigated for 48 h. According to the time-dependent analysis of CHL releasing from $BmiBF_4$/TX-100/water sourced BSA NPs, in the first four hours, CHL was released %15 of the total loaded drug very quickly. However, the drug release rate got slower after that point, and at the end of the 48 h, 24% of the total loaded drug were released (Figure 3.26. A). CHL loaded BSA NPs, which were obtained from $BmimPF_6$/TX-100/water system, also showed a similar trend with BSA NPs from $BmimBF_4$/TX-100/water and released very quick in the first 4 hours (10%), at the end of

the 48 h 12% of total CHL content was released (Figure 3.26. B). The other hydrophilic IL BmimOTf based system BSA NPs released 21% of the loaded CHL content in the first 4 hours and 27% at the end of the 48 hours. The last IL system, $BmimNTf_2$ based synthesized BSA NPs, released 5% of loaded CHL in the first 4 hours and 10% at the end of the 48 hours.

Releasing trends of CHL in all BSA NP types, which were synthesized four different kinds of ILs ($BmimBF_4$, $BmimPF_6$, BmimOTf, and $BmimNTf_2$) and TX-100, exhibited similar kinetics. In the first 4 hours, CHL was released quickly, and releasing rate went down after that.

In characteristics of ILs, a relatively higher amount of chlorambucil (20-25%) was released from the hydrophilic ILs ($BmimBF_4$ and BmimOTf) based BSA NP systems at the end of 48 hours. On the other hand, CHL releasing percentages for hydrophobic ILs, $BmimPF_6$, and $BmimNTf_2$ were 10-12%, respectively.

The hydrophobic ILs ($BmimBF_4$ and BmimOTf) could not form exact microemulsion cores. Nevertheless, the butyl groups of cations of $Bmim^+$ form micelle-like structures.[44] These micelle-like structures enable the water pools to generate BSA NPs.[35,37,38] On the other hand, hydrophobic ILs, $BmimPF_6$, and $BmimNTf_2$, form a microemulsion system, and the water cores act as a nanoreactor to form BSA NPs.[42] As a result of these two formation types, hydrophobic IL-based systems ensure a relatively stable and strict form of BSA NPs than hydrophilic IL comparatively. Hydrophobic IL systems contain higher amounts of surfactant (TX-100) to stabilize the W/IL region of the microemulsion. The BSA NPs from those systems occur in hydrophobic environments, and their surfaces were solidified by crosslinking under that hydrophilic-lipophilic balance conditions. That could make the nanoparticles more hydrophobic. As a hydrophobic drug, CHL, attached to the surface of BSA NP more strictly, and that expected that releasing of CHL might be harder than the BSA NPs from the hydrophilic IL based systems.

3.3.2. In vitro studies of CHL Loaded BSA NPs

Confocal microscopy was used to investigate the cellular uptake of BSA NPs, which were synthesized in $BmimBF_4$, $BmimPF_6$, and BmimOTf based systems. Fluorescein isothiocyanate (FITC) labeled BSA was used to obtain fluorescence active

BSA NPs without change synthesis methods. 0.1 mg/mL FITC-BSA NPs and Huh7 cells (Human hepatoma carcinoma cell line) were incubated for 4 hours and 24 hours for $BmimPF_6$ based system, as described in part 2.3.7. In figure 3.27., confocal microscopy images show that the enclosed FITC-BSA NPs into the cells.

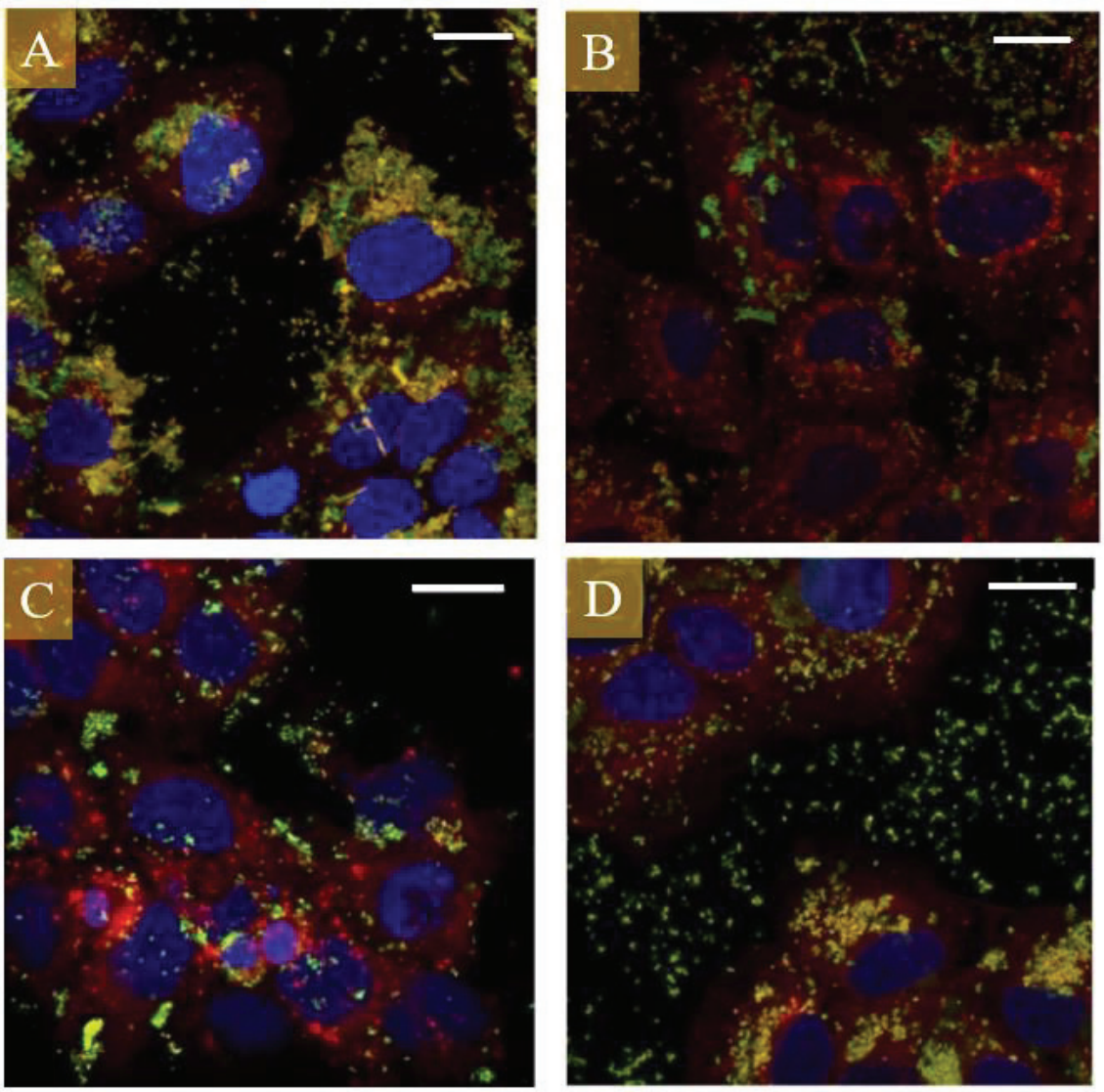

Figure 3.27. Huh7 cells which were incubated FITC-BSA NPs obtained in (A) BmimOTf, (B) $BmimBF_4$, (C) $BmimPF_6$ for 4 hours and (D) 24 hours incubated FITC-BSA NPs from $BmimPF_6$ based system. The cell membranes were stained by DiI (red), and the nuclei were stained by DAPI (blue) (Scale bar is 20 μm).

FITC-BSA NPs (green colors on images) obtained from the BmimOTf system in figure 3.27. (A) were exhibited the most efficiently enclosed nanoparticles depending on confocal microscopy analysis. The BSA NPs located intracellular close to the nuclei in four hours. FITC-BSA NPs obtained from $BmimBF_4$ based system were also endocytosed by the cells, but still dispersed nanoparticles could be seen in the cell medium in figure 3.27. (B). FITC-BSA NPs from $BmimPF_6$ based system were inadequately enclosed in four hours (Figure3.27. (C)). However, the particles were predominantly enclosed in 24 hours of incubation (figure3.27. (D)). Four different types of cell line, MCF7 (human breast cancer cell line), MeWo (Granular fibroblast, human melanoma cell line), Huh-7 (Human hepatoma carcinoma cell line), Hep3B (Human hepatoma cell lines), were used to investigate the effects of CHL loaded BSA NPs which were synthesized in different types of IL-surfactant systems on the cellular viability.

The CHL responses of the cells were also investigated. To understand the effect of CHL on viabilities of the cells, CHL in DMSO solutions was prepared and was added to the cell medium to obtain CHL content up to 320 μM in final concentration (Because of the limited solution of CHL in water 1% DMSO (v/v) were kept constant for each concentration). The procedure was explained in detail in part 2.3.6.

The concentration effects of bare CHL on cell viabilities are shown in figure 3.28. Until 160 μM CHL, no significant necrosis effect of CHL was observed on viabilities. However, Hep3B viability decreased to 50% in the existence of 320 μM CHL showed the most dramatic necrosis rate at that concentration. Consequently, the T-test showed the decrease in cell viability of the Huh-7 cell line at 320 μM CHL as a non-significant. Additionally, the decreased viability of the MCF7 cell line at 160 μM CHL (to 90%) was proved significant by the T-test and showed the most sensitive response to CHL in each concentration. Therefore, Hep3B and MCF7 cell lines were used to investigate CHL-loaded BSA NP effects.

The BSA NPs, synthesized from $BmimPF_6$/TX-100/water system and BmimOTf/TX-100/water system, were chosen to investigate the effects of CHL loaded BSA NPs. However, because of the known toxic effects of BSA NPs from the $BmimBF_4$/TX-100/water system and the relatively larger aggregated particles of BSA NPs from the $BmimNTf_2$/TX-100/water system, these BSA NPs were not used in cellular viability tests.

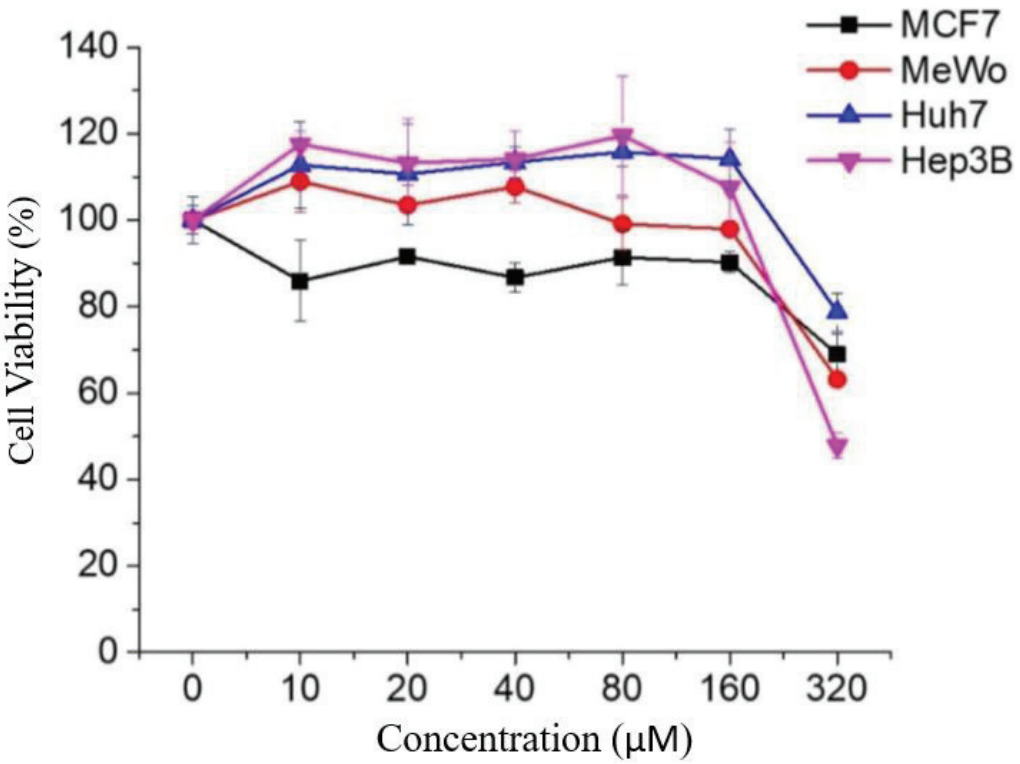

Figure 3.28. Cell viabilities of incubated cell lines of MCF7 (black), MeWO (red), Huh-7 (blue) and Hep3B (pink) with 10, 20, 40, 80, 160 and 320 μM CHL (n=3).

CHL loaded and pure BSA NPs, synthesized in $BmimPF_6$/TX-100/water system, were investigated to define their effects on cell viabilities of the MCF7 cell line at the end of 48 hours and the results were shown in figure 3.29. (B). The pure BSA NPs decreased the viabilities to 85-90% in 0.125, 1.25, and 0.50 mg/mL doses in cell medium. Cell viabilities were decreased to 60% in the existence of CHL-loaded BSA NPs. Even though T-tests did not demonstrate a statistical difference for 0.125 and 0.25 mg/mL CHL loaded BSA NPs, 0.50 mg/mL dose of CHL loaded BSA NPs indicated a significant difference over CHL free, pure BSA NPs.

CHL-loaded and pure BSA NPs, synthesized by BmimOTf/TX-100/water system, were examined for their effects on MCF7 cell viabilities of cell line at the end of 48 hours shown in figure 3.29. A. The pure BSA NPs decreased the viability to 70-80% in each dose in the cell medium. Cell viabilities decreased to 40% in the existence of CHL-loaded BSA NPs. Each dose (0.125, 0.25, and 0.50 g/mL) of CHL-loaded BSA NPs demonstrated a significant effect on MCF7 cell viability against the pure BSA NPs.

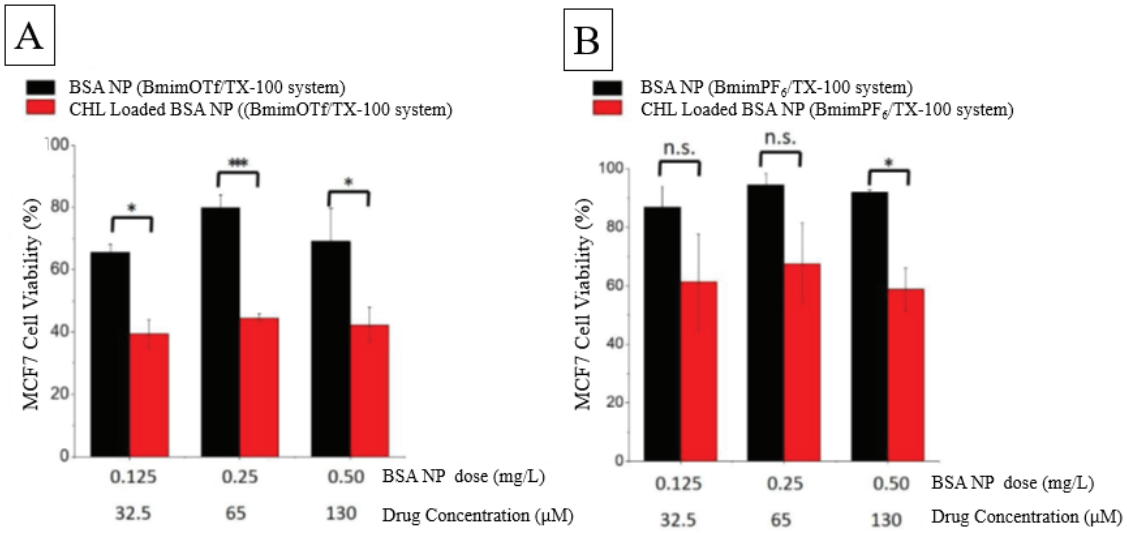

Figure 3.29. The effects of pure BSA NPs and CHL-loaded BSA NPs synthesized in (A) $BmimPF_6$/TX-100/water and BmimOTf/TX-100/water on MCF7 cancer cell line viability (n=3) (n.s.: not significant).

The Hep3B cell viability effects of CHL-loaded and pure BSA NPs, synthesized in the $BmimPF_6$/TX-100/water and the BmimOTf/TX-100/water systems, were shown in figure 3.30. (A) and (B). The pure and CHL-loaded BSA NPs from BmimOTf/TX-100/water system did not indicate a significant difference in studied 0.125, 0.25 mg/mL doses. In contrast, 0.50 mg/mL dose of CHL-loaded BSA NPs demonstrated a notable effect on viability against pure BSA NPs. While pure BSA NPs decreased the viability to 60%, CHL-loaded particles decreased the viability to 40%. On the other hand, pure and CHL-loaded BSA NPs from $BmimPF_6$/TX-100/water system did not significantly affect Hep3B cell viability. In each condition, the cell viabilities decreased to 80%.

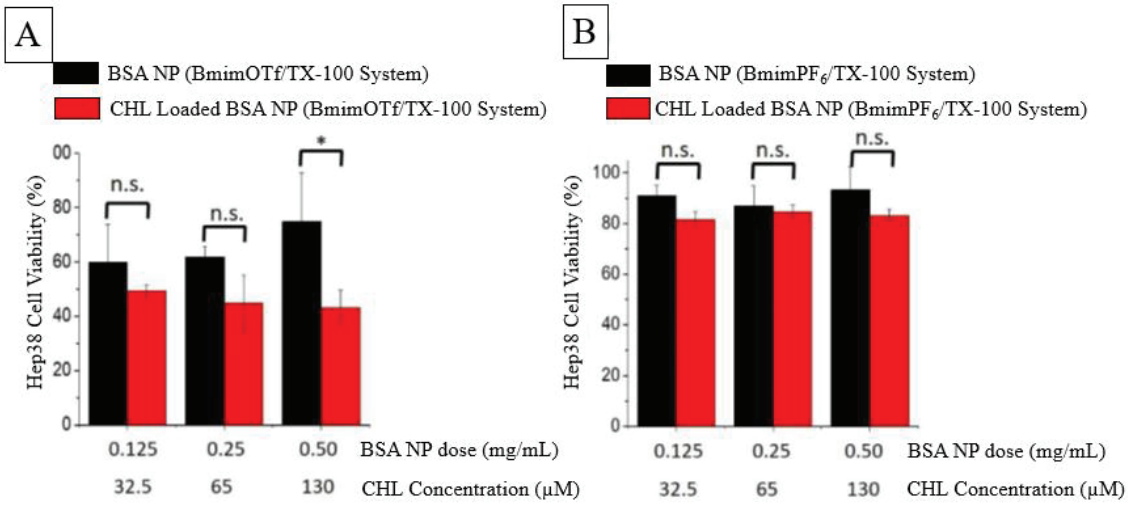

Figure 3.30. The effects of pure BSA NPs and CHL loaded BSA NPs, which were synthesized by (A) $BmimPF_6$/Tween 20/water and (B) BmimOTf/TX-100/water, on Hep3B cancer cell line viability (n=3) (n.s.: not significant).

Due to the low solubility of CHL in water, it is difficult to cellular penetration, which causes cell death in molecular form. Figure 3.28. showed that the free CHL did not remarkably affect cancer cell viabilities in lower doses. However, MCF7 cancer cells were more sensitive to the CHL than other cell lines. Furthermore, the maximum cell death was observed on Hep3B at 320 μM CHL dose. Therefore, investigations were conducted on MCF7 and Hep3B cell lines. In each case, delivering the drug (CHL) by BSA NPs instead of pure CHL demonstrated better performance on the death of cancer cells.

The CHL-loaded BSA NPs of the BmimOTf/TX-100/water system indicated higher toxicity than BSA NPs of $BmimPF_6$/TX-100/water system for both cancer cell lines. While the performance of CHL loaded BSA NPs from BmimOTf/TX-100/water system submitted success for all studied doses for MCF7 cells, only 0.50 mg/mL dose succeeded for Hep3b cell lines. The results of cell viability investigations of BSA NPs of the $BmimPF_6$/TX-100/water system show that the BSA NPs effective only on the MCF7 cell line at 0.5 mg/L dose. Therefore, the performance of the CHL-loaded BSA NPs of the BmimOTf/TX-100/water system makes them a better candidate for drug delivery.

The drug-releasing trend (Figure 3.26.) might be the reason for the better performance of CHL-Loaded BSA NPs of BmimOTf/TX-100/water system in cellular investigations. Higher cell death ratios could cause by the higher amount of released CHL

on that NPs. Despite that, CHL-loaded BSA NPs, synthesized in $BmimPF_6$/TX-100/water system, released the CHL slower and in smaller quantities. These results explain that the BSA NP of the $BmimPF_6$/TX-100/water system does not significantly affect cell viabilities.

CHAPTER 4

CONCLUSION

Besides the known synthesis ways of BSA NPs, BSA NPs were synthesized and optimized in ionic liquid microemulsion systems. Depending on the surfactant-ionic liquid balance, nanoparticles could be obtained in different size distributions and morphology. In addition, the type of the ionic liquid also modifies the properties of the synthesized nanoparticles. In this study, ILs including different types of anions with a common cation, $Bmim^+$, were used to understand their pharmacokinetic potentials on the synthesis of BSA nanoparticles. The type of the used anions of ILs determined the drug loading capacities and releasing dynamics of particles. The water cores of the microemulsion were used as a reactor. The stability of these nanocores affects the size distribution of nanoparticles, which has a crucial role in drug delivery systems. Altering $BmimNTf_2$/TX-100 ratios systematically from 5:90 to 45:50 wt.% in constant 5 wt.% water content decreased the obtained NP size distributions. On the other hand, changing $BmimNTf_2$/Tween 20 ratios from 5:90 to 55:40 wt.% increased the average size of formed BSA NPs with a broader distribution. By changing the weight ratios of IL/surfactant, BSA NPs of average 200-250 nm with a size distribution between 60-400 nm were obtained.

The common pharmaceuticals face some physical and chemical difficulties, such as solubility, diffusibility, non-selective distribution, in every treatment field. This study showed that within the proper parameters, desired size and morphology, adjustable toxicity, and effective drug carriers could be fabricated by using IL-based synthesis methods. Approximately 8-6% CHL loading capacities were found for BSA NPs obtained from $BmimBF_4$, $BmimPF_6$, $BmimNTf_2$ and BmimOTf based systems without significant difference. While 20-25% of loaded CHL released from BSA NPs of hydrophilic BmimOTf and $BmimBF_4$ based systems, 10-12% CHL released from BSA NPs obtained from hydrophobic $BmimNTf_2$ and $BmimPF_6$ based systems.

BSA NPs from the BmimOTf system exhibited enhanced cellular uptake performance over BSA NPs from $BmimPF_6$ and $BmimBF_4$. In four hours BSA NPs obtained from BmimOTf system, NPs dominantly penetrated the cell membranes and located close to the nuclei of the Huh7 cells. Agile drug releasing trend and cellular uptake

ability of BSA NPs from the BmimOTf system may be reason of the improved cytotoxicity effect on MCF7 and Hep3b cancer cell lines. Although free CHL decreased the cell viability to ~90%, the same dose CHL loaded BSA NPs from the BmimOTf system decreased the MCF7 cell viability to ~60% and Hep3b cell viability to ~40% in 0.5 mg/mL BSA NPs concentration.

REFERENCES

(1) Carissimi, G.; G. Montalbán, M.; G. Fuster, M.; Víllora, G. Nanoparticles as Drug Delivery Systems. In *Nanostructured Materials - Classification, Growth, Simulation, Characterization, and Devices [Working Title]*; IntechOpen, 2021. https://doi.org/10.5772/intechopen.100253.

(2) Lohcharoenkal, W.; Wang, L.; Chen, Y. C.; Rojanasakul, Y. Protein Nanoparticles as Drug Delivery Carriers for Cancer Therapy. *Biomed Res. Int.* **2014**, *2014*. https://doi.org/10.1155/2014/180549.

(3) Yih, T. C.; Al-Fandi, M. Engineered Nanoparticles as Precise Drug Delivery Systems. *J. Cell. Biochem.* **2006**, *97* (6), 1184–1190. https://doi.org/10.1002/jcb.20796.

(4) Ahmed, T. A.; El-Say, K. M. Development of Alginate-Reinforced Chitosan Nanoparticles Utilizing W/O Nanoemulsification/Internal Crosslinking Technique for Transdermal Delivery of Rabeprazole. *Life Sci.* **2014**, *110* (1), 35–43. https://doi.org/10.1016/j.lfs.2014.06.019.

(5) Montalbán, M. G.; Coburn, J. M.; Lozano-Pérez, A. A.; Cenis, J. L.; Víllora, G.; Kaplan, D. L. Production of Curcumin-Loaded Silk Fibroin Nanoparticles for Cancer Therapy. *Nanomaterials* **2018**, *8* (2), 7–13. https://doi.org/10.3390/nano8020126.

(6) Fanali, G.; Di Masi, A.; Trezza, V.; Marino, M.; Fasano, M.; Ascenzi, P. Human Serum Albumin: From Bench to Bedside. *Mol. Aspects Med.* **2012**, *33* (3), 209–290. https://doi.org/10.1016/j.mam.2011.12.002.

(7) Spada, A.; Emami, J.; Tuszynski, J. A.; Lavasanifar, A. The Uniqueness of Albumin as a Carrier in Nanodrug Delivery. *Mol. Pharm.* **2021**, *18* (5), 1862–1894. https://doi.org/10.1021/acs.molpharmaceut.1c00046.

(8) Karimi, M.; Bahrami, S.; Ravari, S. B.; Zangabad, P. S.; Mirshekari, H.; Bozorgomid, M.; Shahreza, S.; Sori, M.; Hamblin, M. R. Albumin Nanostructures as Advanced Drug Delivery Systems. *Expert Opin. Drug Deliv.* **2016**, *13* (11), 1609–1623. https://doi.org/10.1080/17425247.2016.1193149.

(9) Saufi, A. N. M.; Ridzwan, N. F. W.; Mohamad, S. Bin; Tayyab, S.; Halim, A. A. A. Fluorometric and Docking Analysis of the Complex Formation between an Anti-Cancer Drug, Chlorambucil and Bovine Serum Albumin. *Indian J. Pharm.*

Educ. Res. **2019**, *53* (4), 682–687. https://doi.org/10.5530/ijper.53.4.131.

(10) Schwarze, B.; Gozzi, M.; Zilberfain, C.; Rüdiger, J.; Birkemeyer, C.; Estrela-Lopis, I.; Hey-Hawkins, E. Nanoparticle-Based Formulation of Metallacarboranes with Bovine Serum Albumin for Application in Cell Cultures. *J. Nanoparticle Res.* **2020**, *22* (1). https://doi.org/10.1007/s11051-019-4708-x.

(11) Kouchakzadeh, H.; Safavi, M. S.; Shojaosadati, S. A. *Efficient Delivery of Therapeutic Agents by Using Targeted Albumin Nanoparticles*, 1st ed.; Elsevier Inc., 2015; Vol. 98. https://doi.org/10.1016/bs.apcsb.2014.11.002.

(12) Sozer, S. C.; Egesoy, T. O.; Basol, M.; Cakan-Akdogan, G.; Akdogan, Y. A Simple Desolvation Method for Production of Cationic Albumin Nanoparticles with Improved Drug Loading and Cell Uptake. *J. Drug Deliv. Sci. Technol.* **2020**, *60* (April), 101931. https://doi.org/10.1016/j.jddst.2020.101931.

(13) Jahanban-Esfahlan, A.; Dastmalchi, S.; Davaran, S. A Simple Improved Desolvation Method for the Rapid Preparation of Albumin Nanoparticles. *Int. J. Biol. Macromol.* **2016**, *91*, 703–709. https://doi.org/10.1016/j.ijbiomac.2016.05.032.

(14) Luebbert, C. C.; Clarke, T. M.; Pointet, R.; Frahm, G. E.; Tam, S.; Lorbetskie, B.; Sauvé, S.; Johnston, M. J. W. Nanoparticle Size and Production Efficiency Are Affected by the Presence of Fatty Acids during Albumin Nanoparticle Fabrication. *PLoS One* **2017**, *12* (12), 1–18. https://doi.org/10.1371/journal.pone.0189814.

(15) Demirkurt, B.; Cakan-Akdogan, G.; Akdogan, Y. Preparation of Albumin Nanoparticles in Water-in-Ionic Liquid Microemulsions. *J. Mol. Liq.* **2019**, *295*, 111713. https://doi.org/10.1016/j.molliq.2019.111713.

(16) Gharbavi, M.; Danafar, H.; Sharafi, A. Microemulsion and Bovine Serum Albumin Nanoparticles as a Novel Hybrid Nanocarrier System for Efficient Multifunctional Drug Delivery. *J. Biomed. Mater. Res. - Part A* **2020**, *108* (8), 1688–1702. https://doi.org/10.1002/jbm.a.36935.

(17) Montalbán, M. G.; Carissimi, G.; Lozano-Pérez, A. A.; Cenis, J. L.; Coburn, J. M.; Kaplan, D. L.; Víllora, G. Biopolymeric Nanoparticle Synthesis in Ionic Liquids. In *Recent Advances in Ionic Liquids*; InTech, 2018. https://doi.org/10.5772/intechopen.78766.

(18) Lei, Z.; Chen, B.; Koo, Y. M.; Macfarlane, D. R. Introduction: Ionic Liquids. *Chem. Rev.* **2017**, *117* (10), 6633–6635.

https://doi.org/10.1021/acs.chemrev.7b00246.

(19) Weingärtner, H. Understanding Ionic Liquids at the Molecular Level: Facts, Problems, and Controversies. *Angew. Chemie - Int. Ed.* **2008**, *47* (4), 654–670. https://doi.org/10.1002/anie.200604951.

(20) Hayes, R.; Warr, G. G.; Atkin, R. Structure and Nanostructure in Ionic Liquids. *Chem. Rev.* **2015**, *115* (13), 6357–6426. https://doi.org/10.1021/cr500411q.

(21) Klähn, M.; Stüber, C.; Seduraman, A.; Wu, P. What Determines the Miscibility of Ionic Liquids with Water? Identification of the Underlying Factors to Enable a Straightforward Prediction. *J. Phys. Chem. B* **2010**, *114* (8), 2856–2868. https://doi.org/10.1021/jp1000557.

(22) Lee, S. H.; Miyauchi, M.; Dordick, J. S.; Linhardt, R. J. Preparation of Biopolymer-Based Materials Using Ionic Liquids for the Biomedical Application. *ACS Symp. Ser.* **2010**, *1038*, 115–134. https://doi.org/10.1021/bk-2010-1038.ch010.

(23) He, Z.; Alexandridis, P. Nanoparticles in Ionic Liquids: Interactions and Organization. *Phys. Chem. Chem. Phys.* **2015**, *17* (28), 18238–18261. https://doi.org/10.1039/c5cp01620g.

(24) Piekart, J.; Łuczak, J. Transport Properties of Aqueous Ionic Liquid Microemulsions: Influence of the Anion Type and Presence of the Cosurfactant. *Soft Matter* **2015**, *11* (46), 8992–9008. https://doi.org/10.1039/c5sm01691f.

(25) Kanwar, R.; Rathee, J.; Tanaji Patil, M.; Kumar Mehta, S. Microemulsions as Nanotemplates: A Soft and Versatile Approach. In *Microemulsion - a Chemical Nanoreactor [Working Title]*; IntechOpen, 2018. https://doi.org/10.5772/intechopen.80758.

(26) Zieliska-Jurek, A.; Reszczyska, J.; Grabowska, E.; Zalesk, A. Nanoparticles Preparation Using Microemulsion Systems. In *Microemulsions - An Introduction to Properties and Applications*; InTech, 2012. https://doi.org/10.5772/36183.

(27) Zhou, G.; Luo, Z.; Fu, X. Preparation of Starch Nanoparticles in a Water-in-Ionic Liquid Microemulsion System and Their Drug Loading and Releasing Properties. *J. Agric. Food Chem.* **2014**, *62* (32), 8214–8220. https://doi.org/10.1021/jf5018725.

(28) Aneesh, T. P.; Rajasekaran, A. Method Development and Validation for the Estimation of Sildosin in Bulk and Pharmaceutical Dosage Forms Using UV-VIS Spectrophotometry. *Asian J. Pharm. Clin. Res.* **2012**, *5* (4), 150–152.

(29) Yordanov, G. G.; Bedzhova, Z. A.; Dushkin, C. D. Preparation and Physicochemical Characterization of Novel Chlorambucil-Loaded Nanoparticles of Poly(Butylcyanoacrylate). *Colloid Polym. Sci.* **2010**, *288* (8), 893–899. https://doi.org/10.1007/s00396-010-2219-5.

(30) Li, G.; Zhao, M.; Zhang, J.; Li, H.; Xu, W.; Pu, L.; Shi, X. Poly(HPMA)-Chlorambucil Conjugate Nanoparticles: Facile Fabrication and in Vitro Anti-Cancer Activity. *New J. Chem.* **2021**, *45* (39), 18544–18551. https://doi.org/10.1039/d1nj03134a.

(31) Hauenschild, T.; Reichenwallner, J.; Enkelmann, V.; Hinderberger, D. Characterizing Active Pharmaceutical Ingredient Binding to Human Serum Albumin by Spin-Labeling and EPR Spectroscopy. *Chem. - A Eur. J.* **2016**, *22* (36), 12825–12838. https://doi.org/10.1002/chem.201601810.

(32) Zhang, Q.; Zhang, L.; Li, Z.; Xie, X.; Gao, X.; Xu, X. Inducing Controlled Release and Increased Tumor-Targeted Delivery of Chlorambucil via Albumin/Liposome Hybrid Nanoparticles. *AAPS PharmSciTech* **2017**, *18* (8), 2977–2986. https://doi.org/10.1208/s12249-017-0782-5.

(33) Tadros, M. I.; Al-Mahallawi, A. M. Long-Circulating Lipoprotein-Mimic Nanoparticles for Smart Intravenous Delivery of a Practically-Insoluble Antineoplastic Drug: Development, Preliminary Safety Evaluations and Preclinical Pharmacokinetic Studies. *Int. J. Pharm.* **2015**, *493* (1–2), 439–450. https://doi.org/10.1016/j.ijpharm.2015.08.011.

(34) Zhang, Q.; Zhang, L.; Li, Z.; Xie, X.; Gao, X.; Xu, X. Inducing Controlled Release and Increased Tumor-Targeted Delivery of Chlorambucil via Albumin/Liposome Hybrid Nanoparticles. *AAPS PharmSciTech* **2017**, *18* (8), 2977–2986. https://doi.org/10.1208/s12249-017-0782-5.

(35) Demirkurt, B.; Akdogan, Y. Development of an Ionic Liquid Based Method for the Preparation of Albumin Nanoparticles. *ChemistrySelect* **2018**, *3* (34), 9940–9945. https://doi.org/10.1002/slct.201801648.

(36) Saihara, K.; Yoshimura, Y.; Ohta, S.; Shimizu, A. Properties of Water Confined in Ionic Liquids. *Sci. Rep.* **2015**, *5*, 1–10. https://doi.org/10.1038/srep10619.

(37) Kattnig, D. R.; Akdogan, Y.; Lieberwirth, I.; Hinderberger, D. Spin Probing of Supramolecular Structures in 1-Butyl-3-Methyl-Imidazolium Tetrafluoroborate/Water Mixtures. *Mol. Phys.* **2013**, *111* (18–19), 2723–2737. https://doi.org/10.1080/00268976.2013.793420.

(38) Kattnig, D. R.; Akdogan, Y.; Bauer, C.; Hinderberger, D. High-Field EPR Spectroscopic Characterization of Spin Probes in Aqueous Ionic Liquid Mixtures. *Zeitschrift fur Phys. Chemie* **2012**, *226* (11–12), 1363–1377. https://doi.org/10.1524/zpch.2012.0272.

(39) Sharma, R.; Mahajan, R. K. Influence of Various Additives on the Physicochemical Properties of Imidazolium Based Ionic Liquids: A Comprehensive Review. *RSC Adv.* **2014**, *4* (2), 748–774. https://doi.org/10.1039/c3ra42228c.

(40) Egan, R. W.; Jones, M. A.; Lehninger, A. L. Hydrophile Lipophile Balance and Critical Micelle Concentration as Key Factors Influencing Surfactant Disruption of Mitochondrial Membranes. *J. Biol. Chem.* **1976**, *251* (14), 4442–4447. https://doi.org/10.1016/s0021-9258(17)33316-1.

(41) Dinarvand, R.; Moghadam, S. H.; Sheikhi, A.; Atyabi, F. Effect of Surfactant HLB and Different Formulation Variables on the Properties of Poly-D,L-Lactide Microspheres of Naltrexone Prepared by Double Emulsion Technique. *J. Microencapsul.* **2005**, *22* (2), 139–151. https://doi.org/10.1080/02652040400026392.

(42) Demirkurt, B.; Cakan-Akdogan, G.; Akdogan, Y. Preparation of Albumin Nanoparticles in Water-in-Ionic Liquid Microemulsions. *J. Mol. Liq.* **2019**, *295*, 111713. https://doi.org/10.1016/j.molliq.2019.111713.

(43) Kelley, B. D.; Wang, D. I. C.; Hatton, T. A. Affinity-based Reversed Micellar Protein Extraction: II. Effect of Cosurfactant Tail Length. *Biotechnol. Bioeng.* **1993**, *42* (10), 1209–1217. https://doi.org/10.1002/bit.260421011.

(44) Akdogan, Y.; Heller, J.; Zimmermann, H.; Hinderberger, D. The Solvation of Nitroxide Radicals in Ionic Liquids Studied by High-Field EPR Spectroscopy. *Phys. Chem. Chem. Phys.* **2010**, *12* (28), 7874–7882. https://doi.org/10.1039/c001602k.